



Facultad
de
Ciencias

Study of the topology of ferroelectric skyrmions

(Estudio de la topología de skyrmiones ferroeléctricos)

Trabajo de Fin de Grado
para acceder al
GRADO EN FÍSICA

Autor: Fernando Gómez Ortiz

Director: Javier Junquera Quintana

Junio - 2018

Dedication

*A los que no es necesario mencionar
porque saben que son todo.
En especial a mi abuelo, estaría orgulloso.*

Acknowledgements

En primer lugar, gracias al departamento de Ciencias de la Tierra y Física de la Materia Condensada por acogerme durante este año y tratarme siempre tan bien. En especial, cómo no, a Javier por enseñarme tanto durante este tiempo y por haber confiado siempre en mí, me ha encantado trabajar contigo. Gracias también a Pablo y Mauro por formar parte de este trabajo y a Antonio y Miguel por contagiarme un poco de su pasión por esta materia.

A mi familia, que siempre esperan de mí lo máximo gracias por el apoyo y cariño durante estos 5 años de largas carreras y por haberme permitido siempre dedicarme a lo que me gusta.

A todos mis compañeros físicos, que pese haberlos abandonado en mi aventura matemática no me han retirado la palabra. Andres, Raquel, Cris, Celia, Unai... gracias por estar ahí siempre. En especial a Elena, creo que necesitaría más páginas de las que ya ocupa este trabajo para agradecerte, gracias por nunca dudar de mí. Ojalá todos me pudieseis ver en traje este Viernes y celebrarlo.

A Nuria Corral y Fernando Etayo, siempre tan dispuestos a echar una mano, gracias por resolverme dudas, por las charlas y por enseñarme tantas matemáticas.

A Andrea y a Gus, gracias por formar parte de lo que soy ahora, por el apoyo, la confianza... ya lo sabéis todo, os quiero mucho.

A Luis, a Hector a Diego, a Javi, a Agus, a la marinera, al team greywolves...

*...A los que estuvieron,
a los que han estado,
a los que, espero, siempre estarán.*

Today I give thanks to everyone who has been part of my life journey, thanks for showing up. I hope you will continue by my side much longer.

Abstract

In the present work, we shall set the basis of a theoretical framework to treat novel complex polarization patterns that arises in Ferroelectric heterostructures, and are ideal candidates to be the ferroelectric counterpart of magnetic skyrmions.

In order to do so, we shall first study magnetic skyrmions, understand the origin of their formation and give a mathematical, more concretely, a topological characterization of its behaviour. Afterwards, we shall try to carry all this knowledge to our ferroelectric case. Finally, we will show that Berry theory is very closely related with many of the aspects treated through this paper and explain its quantum origin.

This work have been carried in collaboration with a phd student of the Luxembourg Institute of Science and Technology, Mauro Gonçalves who was responsible of all second principles simulations of the ferroelectric patterns studied here.

Keywords: Topology, skyrmions, topologically equivalent, vorticity, Skyrmion number, chirality, Berry.

Resumen

En este trabajo, se darán los principios de un marco teórico para entender los patrones de polarización complejos que emergen en heteroestructuras ferroléctricas y son claros candidatos a ser los sustitutos de los conocidos skyrmiones magnéticos.

Para ello, primero, estudiaremos los mencionados skyrmiones magnéticos, entenderemos su origen y daremos una caracterización topológica de su comportamiento. Seguidamente, intentaremos trasladar todo este conocimiento al caso ferroeléctrico. Finalmente, veremos que la teoría de Berry está íntimamente relacionada con muchos de los aspectos tratados en este trabajo y explican su origen cuántico.

Este trabajo se realizó en colaboración con Mauro Gonçalves, estudiante de doctorado del Instituto de Ciencia y Tecnología de Luxemburgo, que realizó las simulaciones de segundos principios de los patrones ferroelectricos estudiados aquí.

Palabras clave: Topología, skyrmiones, equivalencia topológica, vorticidad, número skyrmionico, quiralidad, Berry.

Contents

1	Introduction	1
2	Introduction to magnetic Skyrmions	3
2.1	Mathematical description of a magnetic skyrmion	7
2.2	Topological characterization	7
3	Ferroelectric complex heterostructures.	20
3.1	Introduction: creation of complex textures in ferroelectric materials	21
3.2	Ferroelectric bubbles.	24
3.3	Topological characterization of Ferroelectric bubbles.	26
3.3.1	Order parameter	26
3.3.2	Dimensionality	28
3.3.3	Chirality	29
4	Berry Theory	31
4.1	Classical analogous	31
4.2	Quantum mechanics viewpoint.	34
4.3	Berry physics of magnetic skyrmions	37
5	Conclusions	41
6	Appendix I: Derivation of basic formulas.	44
7	Appendix II: DM interaction revisited.	47
8	Appendix III: Adiabatic theorem and first steps on Berry theory	50
9	Appendix IV: Maths underneath.	53

1 Introduction

In this work we shall combine two different scientific fields that are apparently very far away. Condensed Matter Physics and Topology. Since 2016 when Thouless, Duncan, Haldane and Kosterlitz were awarded with the Nobel Prize of physics, the mixing of these two fields has generated huge interest and it has not reach its zenith.

Topology is the branch of Mathematics that is concerned with the properties that are preserved under continuous mappings. Intuitively these continuous mappings can be thought as deformations (such us expansions, contractions, rotations and so on) but cannot include any kind of cuts or merges.

Two key concepts will be recurrent in this work: “Topologically equivalent” and “Topologically protected”. We shall try here to give some intuitive ideas so that the reader can get more used to this type of terms.

Let’s start with the example schematized in Fig. 1. There we can see a cup and a torus. If you ask someone in the street whether the two objects are the same, the answer will be obviously no. However, for a topologist both objects are homeomorphic, or in other words, they are topologically equivalent. We can continuously deform the cup into the torus and vice versa as it is shown in Fig. 1. In general, we shall say that two mathematical objects such as, surfaces, volumes, vector fields, mappings, and so on are topologically equivalent if there exists continuous mappings that transforms one into the other. Using rigorous mathematical notation, we shall say that two surfaces are homeomorphic, or that the two maps are homotopically equivalent... But all these terms are particularizations of the general idea of two objects that are topologically equivalent.



Figure 1: Topologically, a cup and a doughnut are equivalent: the cup can be continuously deformed into a torus. Reprinted with permission from [1].

The second term “Topologically protected” means that our system is robust under small perturbations such as, thermal fluctuations or applied electric fields. A naïve example that can help us to understand this is the following:

Imagine you want to send an important number to your friend and you have some strips of paper, the easy solution is to write in each strip one digit of the number and send it in order. However this is not a very safe way because the message can be partially erased for example by the rain. Nevertheless, one wise solution is the following: you could write your number in binary and identify the digit “0” with gluing the strip into a cylinder and the digit “1” as a Möbius strip. Using this second possible solution there is no way that environmental noise can turn one digit into another unless you completely destroy the structure.

Topological is just one type of protection. Nevertheless there are others that the reader might be more used to and can help us to understand the concept. For example in the Ising model we have a symmetry breaking protected state that is immutable under small perturbations, we shall introduce it now in order to illustrate what we understand by protected.

Ising model is a very simple mathematical framework to account with collinear magnetism. Within this model, a given material is discretized in a grid. At each point of the grid a vector is defined to represent the local magnetic dipole. These dipoles are restricted to point “up”(↑) or “down”(↓) represented, respectively, by +1 or −1. In order to discuss what we are interested in is enough to consider short-range interactions, more concretely first neighbours interactions. The Hamiltonian of the system takes the following form

$$\mathcal{H} = - \sum_{\langle i,j \rangle} J_{ij} \vec{S}_i \cdot \vec{S}_j,$$

where J_{ij} is a positive constant. For the sake of simplicity, we shall assume that J_{ij} is independent of Temperature and is the same for every pair of magnetic dipoles in the material. The sum extends for $\langle i, j \rangle$ nearest neighbours.

When the temperature is large enough, in particular larger than a critical value T_c , thermal fluctuations permit any random distribution of the spins [Fig. 2(a)] giving rise to an overall magnetization equal to zero, $M = 0$ [Fig. 2(c)]. However when we decrease the temperature until $T = 0K$ thermal fluctuations vanish and the system adopts its minimal energy state where all the spins are aligned parallel. However because of the symmetry of our Hamiltonian to the change $\vec{S} \rightsquigarrow -\vec{S}$ in principle our system can adopt two different degenerated states the one with $M = 1$ and the one with $M = -1$. [Fig. 2(b)]

As both states are degenerated in energy [Fig. 2(d)], both are equiprobably accessible. However, if the system is large enough, once the system adopts one of the states, let's say $M = 1$, it is statistically impossible to transit to the state $M = -1$ unless very strong perturbations are realised to the system, for instance by an external magnetic field or an

increase in the temperature.

In this sense the system $M = 1$ is protected, and our system has broken one symmetry of our initial Hamiltonian. It is important to notice that protected does not mean immutable, if we give the system enough energy to surpass the potential barrier we can make a transition to the other state.

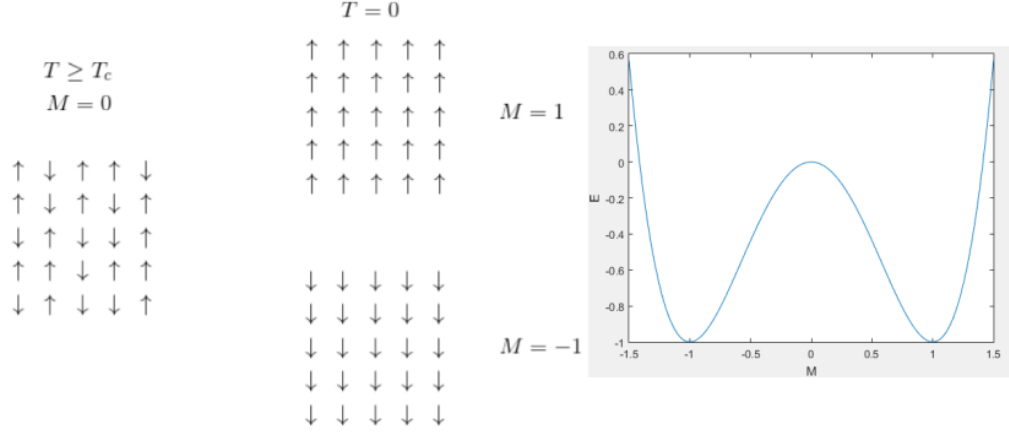


Figure 2: Ising model of a Ferromagnet. The arrows schematically represent the allowed value of the local magnetic dipoles in a discretized two-dimensional square lattice. (a) disordered configuration due to large thermal fluctuations. (b) Degenerate ground states at $T = 0$ K. (c) Magnetization M as a function of temperature. (d) Energy as a function of temperature.

2 Introduction to magnetic Skyrmions

The Ising model discussed up to this point is a classical textbook example to describe some of the most technologically important magnetic materials. However, the last decade has seen the explosion of more fancy magnetization patterns known as skyrmions.

Magnetic skyrmions are topologically protected whirling spin textures such as the one schematically pictured in Fig. 3. These complex magnetic textures can be stabilized in magnetic materials by an asymmetric exchange interaction, not present in the previous Ising model, between neighbouring spins that imposes a fixed chirality [2]. They can be described as a vector field with the following properties.

1. *All the vectors point along a given direction at the external surface of the skyrmion (vectors plotted in red in Fig.3, pointing in the positive direction.)*

2. *The vectors point in the opposite direction at the centre of the skyrmion (vectors plotted in blue in Fig.3, pointing in the negative direction.)*
3. *In the intermediate region the vector field rotates in a continuous way.*

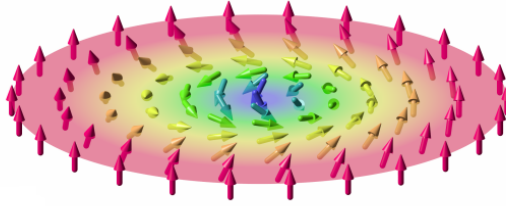


Figure 3: Schematic representation of a combed hedgehog magnetic skyrmion. Reprinted with permission from [3].

Their small size, of the order of 90 nm, together with the robustness against external perturbations, make magnetic skyrmions potential storage bits in a novel generation of memory and logic devices [4].

Recent studies show promise for the application of the skyrmion to non-volatile magnetic memory, which has the advantages of low driving current and high memory density over the magnetic bubble and racetrack memory devices [5].

Their nature cannot be explained with the basic Ising model for ferromagnetic materials explained above. In order to ascertain the origin of the whirling patterns we have to take into account two different interactions.

The first one is the exchange coupling which is responsible of the ferro- or antiferromagnetism. In this work we will refer to it as the symmetric part of our Hamiltonian because the transformation ($\vec{r} \rightsquigarrow -\vec{r}$ i.e. inversion) remains this part of the Hamiltonian invariant. Its mathematical expression for a pair of spins \vec{S}_1 and \vec{S}_2 is

$$\mathcal{H}_{sym} = -J \cdot (\vec{S}_1 \cdot \vec{S}_2).$$

The second one is the Dzyaloshinskii-Moriya (DM) [6, 7] interaction that arises in systems with strong spin-orbit coupling. We shall call this interaction the antisymmetric Hamiltonian because the transformation ($\vec{r} \rightsquigarrow -\vec{r}$) reverse its sign. Its mathematical expression for a pair of spins \vec{S}_1 and \vec{S}_2 is

$$\mathcal{H}_{asym} = -\vec{D}_{12} \cdot (\vec{S}_1 \times \vec{S}_2).$$

Where the vector \vec{D}_{12} measure the interaction between the two spins and depends on the material and the distance between them. The vector \vec{D} has some interesting properties that are fundamental for the understanding of the interaction and are explained below. Notice that if we perform the so called inversion then \vec{D}_{12} change its sign as we picture schematically in Fig 4.

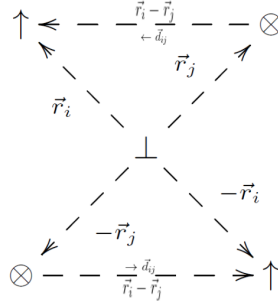


Figure 4: Schematic view of how inversion reverses the sign of the DM interaction vector

Hence, as we anticipated before, even if the product $\vec{S}_1 \times \vec{S}_2$ remains invariant under the transformation, our Hamiltonian reverses sign. This implies for instance, that systems with an inversion symmetry with respect to the centre of the two magnetic spins are not allowed to present this interaction.

Another interesting property of the vector is its dependence with direction that makes it anisotropic. For physical reasons $\mathcal{H}_{asym12} = \mathcal{H}_{asym21}$ because we are measuring the energy of the system in two different frames, and therefore, it must be invariant. If we impose this condition we arrive to the property

$$\begin{aligned} \mathcal{H}_{asym12} &= -\vec{D}_{12} \cdot (\vec{S}_1 \times \vec{S}_2) = -\vec{D}_{21} \cdot (\vec{S}_2 \times \vec{S}_1) = +\vec{D}_{21} \cdot (\vec{S}_1 \times \vec{S}_2) \Rightarrow \\ \vec{D}_{21} &= -\vec{D}_{12} \end{aligned}$$

The direction of the vector \vec{D}_{ij} can lie either parallel or perpendicular to the line connecting the two spins with the exact direction depending on the symmetry of our system [8]. The Hamiltonian that our system obeys is the balance between both interactions and has the form

$$\mathcal{H} = \mathcal{H}_{sym} + \mathcal{H}_{asym} = -J \cdot (\vec{S}_1 \cdot \vec{S}_2) - \vec{D}_{12} \cdot (\vec{S}_1 \times \vec{S}_2).$$

As it is schematized in [Fig. 5(a)] when we only consider the symmetric part, ferro or antiferro ordering arises because the system with lowest energy is the one where spins are coupled parallel or antiparallel depending on the sign of J . However, if we only consider

the DM interaction, [Fig. 5(b)], the energy is minimized for a configuration where neighbouring spins are orthogonal.

When both interactions take part in the overall Hamiltonian a compromise between both extreme cases must be achieved. In order to minimize energy, the system cants neighbour spins and provoke whirling textures such as the skyrmions or the ones depicted in [Fig. 5(c)].

Naturally, depending on the orientation that the vector \vec{D}_{ij} presents we shall end up having different results that are physically distinguishable.

When the vector \vec{D}_{ij} lies parallel to the line connecting both spins the pattern shall look like the helix schematically represented in [Fig. 5(c.1)]. This helical state is chiral and so we can attach to it a handedness. The helix in Fig. 5(c.1) is right-handed. Depending on the sign of \vec{D}_{ij} the handedness shall change. However, when the vector \vec{D}_{ij} lies orthogonal to the line connecting both spins the resulting pattern exhibits no chirality as it is pictured in [Fig. 5(c.2)]. Those states are hence physically distinguishable.

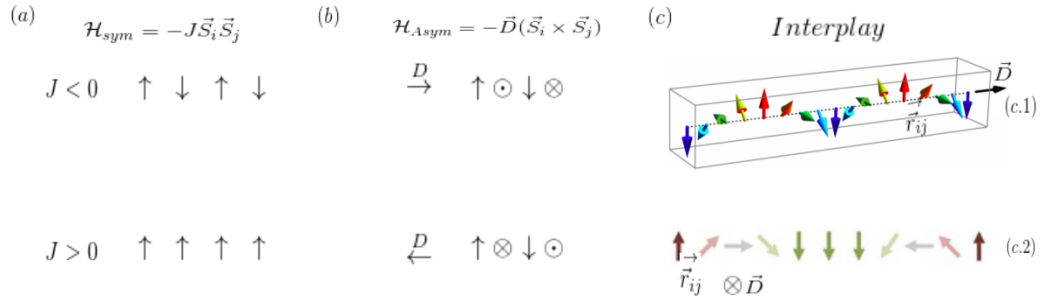


Figure 5: (a) Contribution of the symmetric Hamiltonian that tends to align parallel or antiparallel neighbour spins depending on the sign of the constant J . (b) DM interaction that tends to cant neighbour spins orthogonally. Depending on the direction of the vector \vec{D}_{ij} chains of spins rotate differently. (c) Interplay between both interactions that tends to cant neighbour spins. (c.1) chiral helical state that arises when the DM vector lies parallel to the line connecting the two spin sites. (c.2) non chiral phase that arises when the DM vector lies orthogonal to the line connecting the two spin sites.[9]

For a deeper analysis of the DM interaction effect in our system of spins check Appendix II.

2.1 Mathematical description of a magnetic skyrmion

Magnetic skyrmions are typically formed at the interface in B20-type silicides and germanides where the interplay between strong spin-orbit interaction and ferromagnetism is present[10]. Therefore, the vector field of local magnetic moments is defined in a $2D$ -plane. It is important to note, that despite the fact that the position of a local spin is defined in $2D$, the spin itself can point in any direction of the three dimensional space, as clearly depicted in Fig 3.

Mathematically, the spin textures can be described using a vector field of the form[11]

$$\vec{n}(\vec{r}) = (\cos \Phi(\phi) \sin \Theta(r), \sin \Phi(\phi) \sin \Theta(r), \cos \Theta(r)), \quad (1)$$

where $\vec{n}(\vec{r})$ is a normalised $3D$ vector defined in a $2D$ space and $\Phi(\phi)$ and $\Theta(r)$ are functions of the azimuthal angle ϕ and distance r (polar coordinates that describe the position \vec{r} where the local spin is located). Particular functional forms will depend on the specific pattern to be described, some of them will be discussed later on.

The vector \vec{n} can be thought to be our order parameter. In magnetic skyrmions \vec{n} represents the local magnetic moment. We shall replace latter in this work the magnetic dipole by the electric polarization in complex ferroelectric textures. The Berry theory will be underneath its behaviour as we shall explain in Sec. 4.

2.2 Topological characterization

Now that we have parametrized our magnetic skyrmions as Eq. (1) states we are able to study its topological properties as a vector field defined in a surface (xy -plane).

As a first step we shall try to characterize this type of patterns simplifying the problem and projecting the order parameter in the xy -plane. In other words, we shall first study the tangent component of our vector fields. A few patterns of the different possible tangent vector fields are presented in Fig. 6

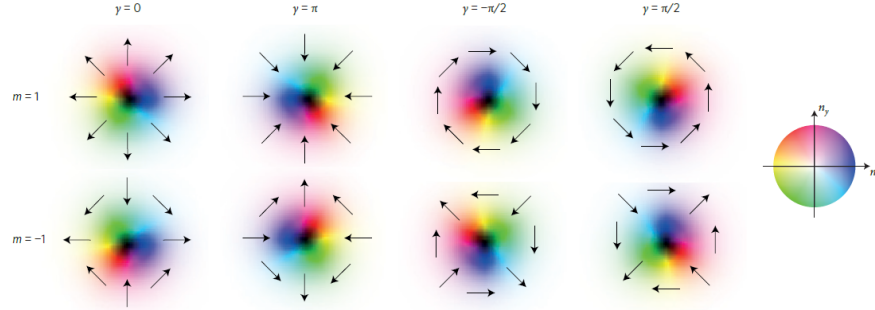


Figure 6: Different possible arrangements for magnetic textures in terms of m and ϕ . Arrows represent the direction of the order parameter at given positions. These directions are also indicated by the colour map according to the caption shown by the circle at the right[11].

Where m stands for vorticity and measure how much our pattern rotate and γ indicates the initial angle that our vector field makes with the axis x . Proper definitions will be given in this section later on.

Some of the vector fields of Fig. 6 are topologically equivalent and some are not, in advance, we shall show that vector fields with the same number m will be equivalent. In order to have a definition for the number m and study this topological equivalence we will first give some basic definitions.

We say that a tangent vector field \vec{v} defined on a surface S presents a singularity if for some point of its domain $x \in S$, it holds that $\vec{v}(x) = 0$. The reason why we call them singularities can be understood if we think the vector field as “velocity curves”. Because of Cauchy theorem of uniqueness and existence of solution in differential equations given a direction and a point we only have one integral curve. However, when the vector field vanishes we do not have any information about the integral curves. Through that point it may pass zero, one or infinite (vortex, dipole, source) integral curves. Mathematically these points are singular in the sense that they are rare, we need to study its neighbourhood in order to understand them. Moreover, singularities also usually lead to discontinuities of the vector field as it is shown in Fig. 7. As we approach as much as we want to the origin marked with a cross, the vector field cant go continuously from the value it takes on a point to the value it takes on its antipodal pair and so it presents a discontinuity on $(0, 0)$.

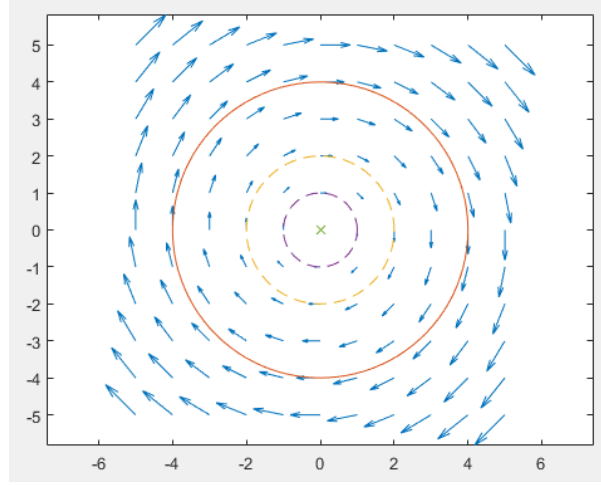


Figure 7: Vector field with a singularity in the origin. This point is also a discontinuity of our vector field.

Physically those points are interesting because singularities will correspond to defects of our material. In this work we shall focus on point-like defects. However, higher dimensional defects are also recurrent in condensed matter and can be studied with techniques similar to the ones developed in this work.

We shall define index of the singularity $I(v, x)$ or equivalently, vorticity of the vector field m at the point x as the number of times that the vector field wraps the unit sphere \mathbb{S}^1 of radius ϵ centred in x . The degree of the vector field will be the sum of the indexes of all its singularities $\deg(v) = \sum_{x \in \text{Sing}} I(v, x)$ and can be thought to be the global vorticity of the vector field. We can see a sketch of how to compute this index in Fig. (8).

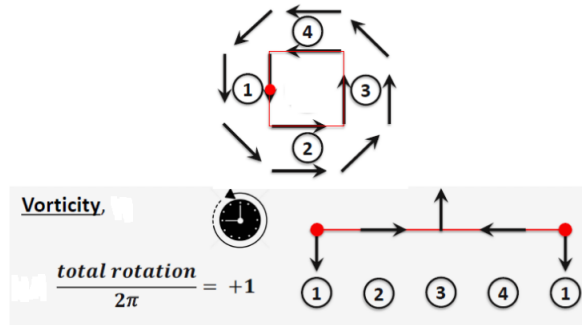


Figure 8: As we move counter-clockwise the unit sphere our vector field moves also counter-clockwise. This sense of rotation will be taken as positive.

Counting with the criteria of signs described in the Fig. 8, the index will be the number of turns that the vector field does in just one turn to the unit sphere.

It can be mathematically proved that the index of the vector field is independent of the choice of the radius of the sphere along the one we do the calculus as long as it only contains one isolated singularity. Doing that exercise to all the vector fields of Fig. (6) we can fill the following table.

Vector field	vorticity
$m = 1, \gamma = 0$	1
$m = 1, \gamma = \pm\frac{\pi}{2}$	1
$m = 1, \gamma = \pi$	1
$m = -1, \gamma = 0$	-1
$m = -1, \gamma = \pm\frac{\pi}{2}$	-1
$m = -1, \gamma = \pi$	-1

Table 1: Vorticity for some the fields described in Fig. (6). As it was expected from the definition m fits vorticity values.

It is important to warn the reader that despite the fact that in this examples indexes are only taking the values ± 1 it also can be 0 for the constant field where we do not have singularities for example, or arbitrarily high for other type of patterns. We shall discuss this in a few moments, but first lets see a result that will tell us when two vector fields are homotopically equivalent¹.

We have the following result proved by Hopf: “*Two vector fields are topologically equivalent if and only if they have the same degree*”. This means that we can continuously go from any of the vector fields to another if they share the same row of Fig. 6. Intuitively we only have to rotate all the vectors a constant factor $\gamma_1 - \gamma_2$. In this way γ is defined as the angle that the vector field makes with the horizontal axis. In addition, the theorem also allows us to say that it does not exist any continuous function that will take one vector field of the first row into any of the second row.

We have that the index satisfies the following property: If a contour include two singularities P and Q the index of the vector field along the contour will be the sum of the indexes of two independent contours one including each of the singularities because, as Fig. 9 shows we can continuously deform one contour into the other.

¹This means that both can be related by continuous functions

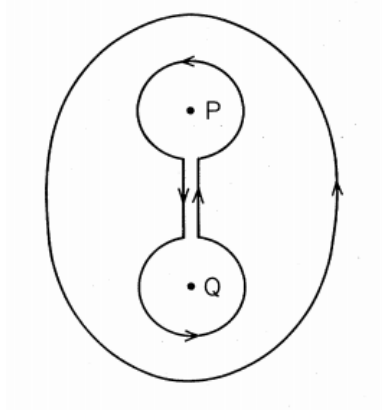


Figure 9: Two point singularities P and Q and two surrounding contours. The index on the inner contour is the sum of the indexes determined by P and Q separately. Since the inner contour can be continuously deformed into the outer one, this is also the index for the outer contour. [12]

In particular, a vector field with two singularities x and y such that $I(v, x) = +1$ and $I(v, y) = -1$ will be topologically equivalent to the constant field even if one has 2 defects and the other has none. Moreover as we anticipated before, merging singularities of index 1 we can create fields with arbitrarily high degree. For example in Fig. 10 we can see a vector field with degree 2.

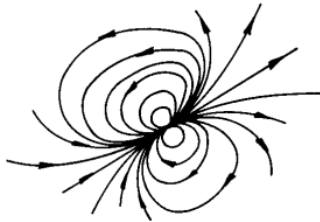


Figure 10: Singularity of index 2.[13]

However, when we are working in a crystal we are imposing periodic boundary conditions and so we are identifying edges of the unit cell, this means that we are working in the topology of the torus (\mathbb{T}^2) as it is depicted in Fig. 11.

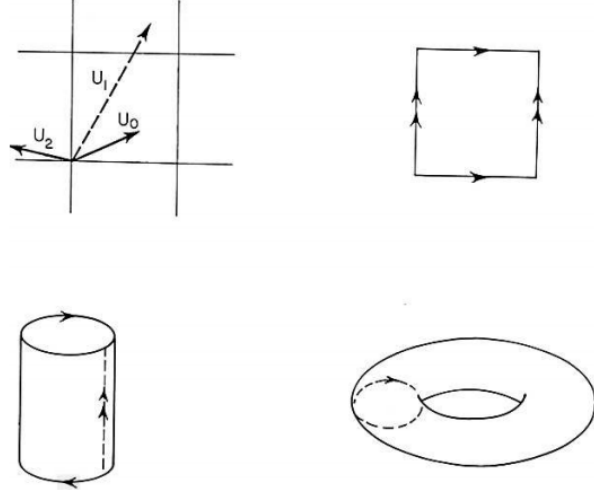


Figure 11: Scheme of how periodic boundary conditions induce the topology of the torus in our unit cell.[14]

As a consequence of Poincaré-Hopf theorem, all tangent vector fields defined in the surface of a Torus must have degree zero which coincides with its Euler characteristic². Lets study what happen exactly when we impose periodic boundary conditions when for example we have a single singularity of $m = 1, \gamma = \frac{\pi}{2}$.

In Fig. 12 we show an schematic view of how new singularities appear, in the corners of the unit cell they appear singularities of index 1 apart from the one in the centre of the unit cell that was the original. In the middle of the edges we have singularities of index -1 adding all of them up we get:

$$1 + \frac{1}{4} \cdot (1 + 1 + 1 + 1) - \frac{1}{2}(1 + 1 + 1 + 1) = 0$$

Where we divide by $\frac{1}{4}$ or $\frac{1}{2}$ depending on the number of unit cells that share the same singularity.

²We remember that the Euler characteristic of a triangulable surface is defined as $\chi(S) = v - e + f$ where v , e , f stands for vertex, edges and faces of any triangulation.

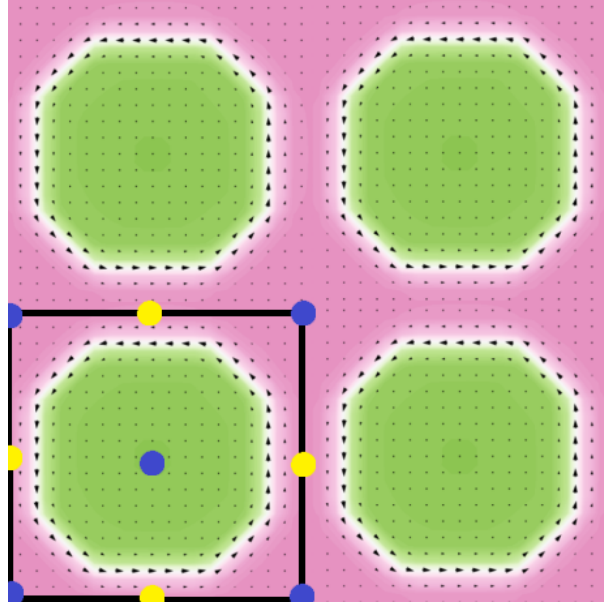


Figure 12: Scheme of how periodic boundary conditions induce the creation of new singularities. Blue points stand for singularities of index $+1$, whereas yellow ones stands for singularities of index -1 .

This is not a proof for the general case but as Poincaré-Hopf states, our vector field has degree zero. This means that analysing the simplified problem without the z component of our order parameter wont let us to distinguish between the two following patterns shown in Fig. 13. Nevertheless, we would be interested in differentiate both patterns since pattern in (a) present a defect where as the pattern in (b) presents no defects.

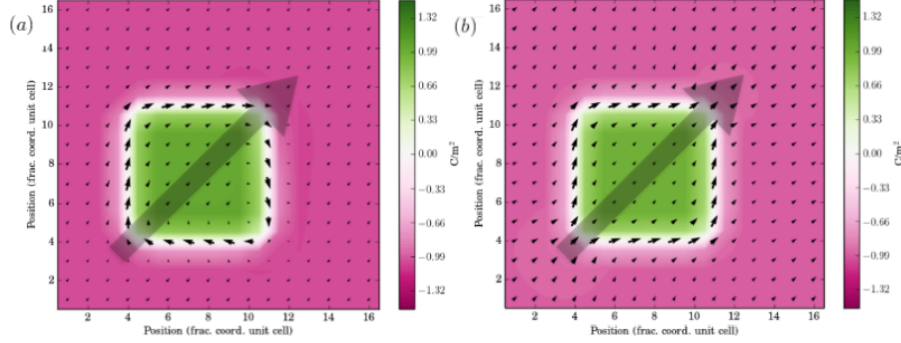


Figure 13: Two different patterns that are indistinguishable after periodic boundary conditions in terms of vorticity. In (a) Skymionic pattern that presents vorticity $m = 0$ when periodic boundary conditions are imposed. In (b) monodomain pattern that presents also vorticity $m = 0$. We will need higher dimensional topological invariants in order to distinguish them.

In order to solve this problem we shall need a higher dimensional topological invariant which is the Pontryagin density or Skymion number defined as

$$N_{sk} = \frac{1}{4\pi} \int \int d^2r \cdot \vec{n} \cdot \left(\frac{\partial \vec{n}}{\partial x} \times \frac{\partial \vec{n}}{\partial y} \right). \quad (2)$$

This is the higher dimension equivalent and counts the number of times that the vector field wraps the unit sphere(\mathbb{S}^2).

If we want to topologically distinguish patterns with defects we need the information of the third component of our order parameter. If we compute now the Skymion number of the two fields above we will get that $N_{sk} = 1$ for the first field and that $N_{sk} = 0$ for the second one and, as one would expect we will be able to distinguish between the two mappings.

Now that we know that the Skymion number is a good way to characterize different patterns we will learn how to compute it in a easy way. After all the calculus developed in Appendix I we have proved that the Skymion number can be computed as

$$N_{sk} = \frac{1}{4\pi} [-\cos \Theta(r)]_0^\infty [\Phi(\phi)]_0^{2\pi} \quad (3)$$

Lets study first the meaning of the second and “difficult” part of the integral $[\Phi(\phi)]_0^{2\pi}$. This, according to the expression of our order parameter Eq. (1) will be proportional to the number of times that the in-plane component of our vector field wraps \mathbb{S}^1 lets see

what this constant should be.

If we take the universal covering of the unit sphere

$$\begin{aligned}\Psi : \mathbb{R} &\longmapsto \mathbb{S}^1 \subset \mathbb{C} \\ t &\longmapsto e^{i2\pi t}\end{aligned}$$

we have that the path $\alpha(t) = t$, with $t \in [0, 1]$ lifts to the path that gives only one turn to the unit sphere, as our parameter ϕ can take values in the interval $[0, 2\pi]$ we have the following relation,

$$m = \frac{[\Phi(\phi)]_0^{2\pi}}{2\pi}. \quad (4)$$

We can now completely understand the functional form of $\Phi(\phi)$ it will be described as $\Phi(\phi) = m\phi + \gamma$ where γ will be the initial angle that the spins make with respect to the horizontal. In particular, it will also relates two fields v_1, v_2 of the same vorticity with a rotation of $\gamma_1 - \gamma_2$ radians.

The first part of the integral $[-\cos \Theta(r)]_0^\infty$ is more easy and just count how the third component of our order parameter has change. Hence we have an easy recipe to compute the Skyrmion number $N_{sk} = \frac{1}{2} [-\cos \Theta(r)]_0^\infty \cdot m$ if our order parameter points down at $r \rightarrow \infty$ and up at $r = 0$ then we have that $N_{sk} = m$ and if at $r \rightarrow \infty$ and $r = 0$ it points in the same direction then $N_{sk} = 0$ no matter what value takes the vorticity. Patterns where the order parameter points up in $r = 0$ and are tangent to the xy -plane at $r = \infty$ are called *merons* and have semi-integers topological numbers.

As a final note, and in parallelism with what we did in the two-dimensional case we shall make a table labelling different patterns shown in Fig. 14 in terms of its Skyrmion number, and will try to give a intuitive idea to the phrase “wraps the sphere \mathbb{S}^2 ”.

Pattern	N_{Sk}
Hedgehog antiskyrmion	-1
Hedgehog Skyrmion	+1
Bloch-antiskyrmion	-1
Bloch-Skyrmion	+1

Table 2: Skyrmion number for different patterns.

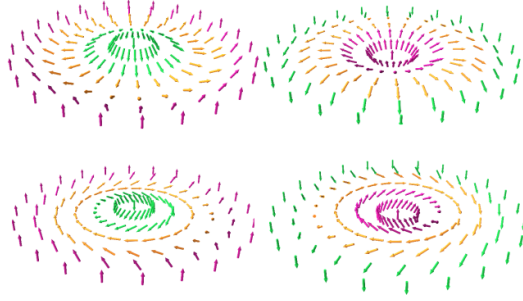


Figure 14: Different types of patterns from top to bottom, left to right, Hedgehog anti-skyrmion, Hedgehog skyrmion, Bloch-antiskyrmion, Bloch-Skyrmion.[15].

In Fig. (15) we show the intuitive idea of wrapping the sphere seeing the pattern as the stereographic projection of a vector field defined on the sphere. There exists therefore a bijection between the pattern defined in the unit sphere and the “extended” pattern in the xy -plane, we shall say that the so-called pattern wraps the unit sphere if its bijected representative do so.

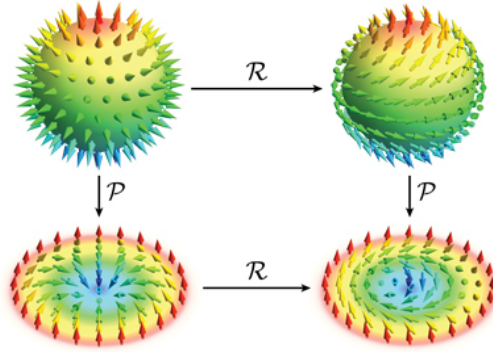


Figure 15: Different patterns of $N_{sk} = -1$ that wraps the sphere once. Reprinted with permission from [16].

Is important to realize that what we are studying is the topology of our order parameter space, that is to say, the space where our order parameter moves on. In the case were we neglected the third component of $\vec{n}(\vec{r})$ this space was the sphere \mathbb{S}^1 whose first homotopy

group is $\pi_1(\mathbb{S}^1) \cong \mathbb{Z}$.

This identification of our order parameter space is obvious because we have unitary vectors that can point anywhere in the plane and so, we bijectively map any unitary vector with a point in \mathbb{S}^1 , considering for example the angle our vector makes with the horizontal axis and associate it with the point $e^{i\theta}$ in the sphere as it is schematized in Fig. 16.

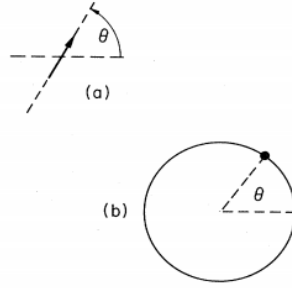


Figure 16: (a) Planar unitary vector in a given direction. (b) The representation of that direction in the order parameter space. [12]

When we start considering the third component our order parameter space, it now becomes a sphere \mathbb{S}^2 whose first homotopy group is trivial and it holds $\pi_2(\mathbb{S}^2) \cong \mathbb{Z}$. We can map any pattern described by our vector field into a vector field defined on our order parameter space as it is shown in the example of Fig. 15. Hence, as it holds that $\pi_n(\mathbb{S}^n) \cong \mathbb{Z}$ it is not surprising that the dimensionality of our topological invariant increase with the dimensionality of the order parameter space if we are working with sphere-type spaces.

In all this section we have learned how to characterize different patterns from a topological point of view, in particular we have seen that all these numbers are topological invariants and so they are preserved under any continuous deformation, so they are robust under small changes in Temperature for example.

As a final note to this section, we will study a very interesting and potentially applicable property of Skyrmions, they can present Chirality.

Chirality is a type of asymmetry that makes an object distinguishable from its mirror image. Mathematically, we say that a object is chiral if it can not be mapped to its mirror image by rotations and translations.

It can be proved that chiral objects have a non zero Helicity integral: $H = \int \int_S \vec{n}(\vec{\nabla} \times \vec{n})$

and that the sign of the integral is opposite for its enantiomer. As it is proved in Appendix I, this integral can only be non zero in skyrmionic patterns such as the ones we are studying with $m = 1$ and $\gamma \neq k\pi$ with k integer. As a consequence of this, we will only expect chirality in $m = 1$, $\gamma \neq k\pi$ skyrmions.

In Fig. 17 we show two chiral skyrmion pairs. Both patterns share the same N_{Sk} but to the first one we can attach a left hand whereas the second one is right handed.

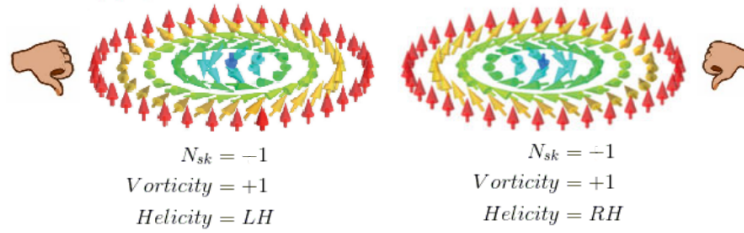


Figure 17: Chiral pair of Skyrmions.[17].

An easy and naïve way to see the chiral state of an object without computing the integral is to whirl the fingers of your hand in the direction of the in-plane vectors. This will determine the direction of the third component as the direction of your thumb. The hand that fit the pattern is the handedness of the chiral state.

Again, in order to present chirality is essential to take into account the third component of our order parameter, if we avoid this component we can not attach any handedness to our objects. In Fig. 18 we have schematized both vector fields that we are studying. If we neglect the z component both vector fields are related by the rotation of π degrees around the z -axis. Nevertheless, when we include the third component of our order parameter this does no longer hold and so chirality appears.

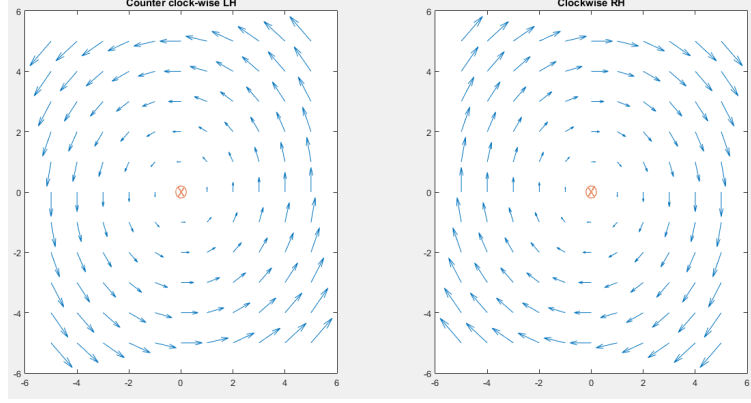


Figure 18: Schematic vision of the vector fields of Fig. 17 in a neighbourhood of the singularity.

What is interesting to note here is that both chiral states presents the same Skyrmion number ($N_{sk} = -1$) and as a consequence, both states are related by a continuous deformation, we do not have any topological barrier to go from one into the other and so we should be able to control and change the chirality of our patterns with the action of external magnetic fields. This fact open the door for the appliance of this structures in memory devices or other optical applications.

However, we can also have chirality in Skyrmions with $N_{sk} = +1$, in fact we can have two right-handed skyrmions with equal vorticity but opposite skyrmion number, such as the ones that are depicted in Fig. 19. In this case, if we try to transform one into the other by changing the out of plane component of our order parameter we will pass through a critical point as it was expected -I remind that having different N_{sk} implies that the transformation cannot be continuous-. Nevertheless, if we perform this discontinuous transformation we will realize that when the skyrmion goes from $N_{sk} = +1 \rightsquigarrow N_{sk} = -1$ it also changes its chiral state form $RH \rightsquigarrow LH$, hence, right-handed skyrmions are somehow related (by a discontinuous deformation) with left-handed anti-skyrmions.

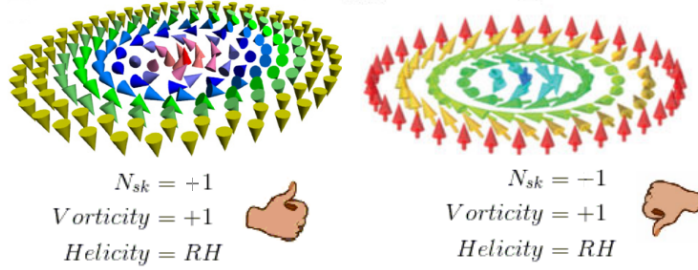


Figure 19: Chiral anti-skyrmion skyrmion in the same chiral state.[17]

In conclusion what we obtain is that Skyrmion chirality is not topological because we can have both chiral states without changing its topological characterization which is the skyrmion number. It is proved that chiral states are due to Dzyaloshinskii-moriya interaction whose Hamiltonian is described by Tokura as:

$$H_{DM} = DM \cdot \vec{n} \cdot (\vec{\nabla} \times \vec{n}).$$

As in the Appendix I we have seen that this Hamiltonian presents the form Eq. (16), depending on the sign of the constant DM we will have that the lowest energy will be achieved for $m = 1$ and $\gamma = \pm \frac{\pi}{2}$ that is to say, either the right or left handed chiral state. See Appendix II for a deeper analysis of the DM interaction.

In order to go from one state to another we have to surpass DM-barrier.

3 Ferroelectric complex heterostructures.

In Sec. 2 we have mathematically characterized complex topological vector field patterns in terms of an order parameter that satisfies certain restrictions. Theory was illustrated with examples borrowed from the study of magnetic skyrmions. Here we shall extend it to the case of ferroelectric complex patterns of the electric dipole.

Many natural structures exhibit chirality and present topological phases that are essential to their functional interactions, yet the chiral electronic structures found in condensed matter systems have been primarily limited to magnetic materials. The electric dipole equivalent of magnetic skyrmions has remained conspicuously elusive. However, new theoretical predictions and experimental observations of the continuous rotation of electric polarization in titanate superlattices suggest that such materials are ideal candidates to present equivalent properties [18]. Some of the recent theoretical and experimental progress are exposed in Fig. 20

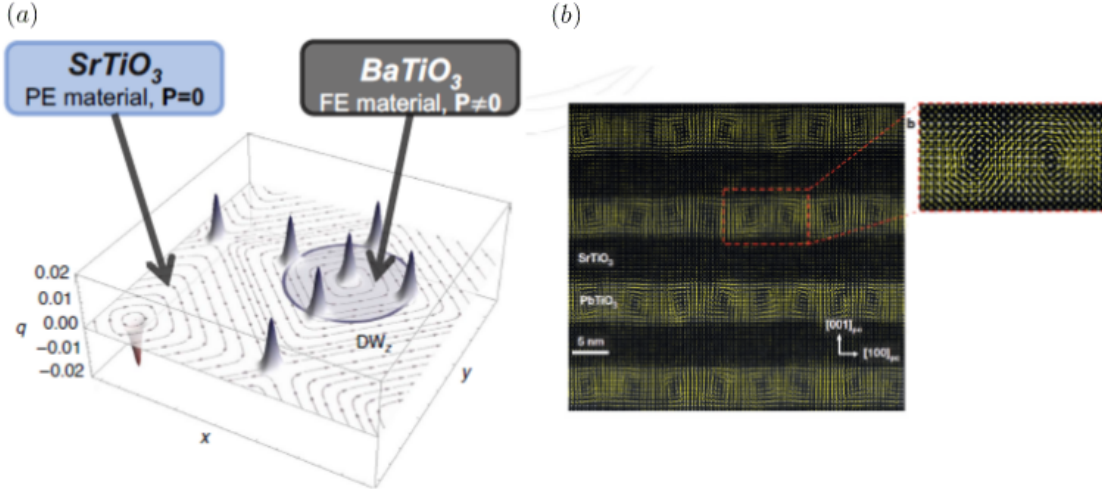


Figure 20: Topologically non trivial textures in ferroelectric materials. In (a) first theoretical prediction using calculation. It is composed of a $BaTiO_3$ nanowire embedded in a $SrTiO_3$ matrix and it present vortex-like polarization in plane with an out of plane normal component which turn it into an optical active material. In (b) rotational textures found experimentally in $PbTiO_3/SrTiO_3$ superlattices observed with transmission electron microscopy. The structure is characterized by the spontaneous formation of laterally alternating clockwise and counterclockwise vortices of electric polarization.[19, 20]

3.1 Introduction: creation of complex textures in ferroelectric materials

In this section we shall try to introduce the origin of complex topologies and vortex-like structures that arise in thin films or at the interfaces of ferroelectric materials.

It is well known from basic electrostatics that discontinuities of the polarization at a surface originates an accumulation of bound charges as the following relation states

$$\vec{\nabla} \cdot \vec{P} = -\rho_b.$$

If we dispose of a bulk ferroelectric material ($PbTiO_3$ for example), the phase of minimal energy will be the polarized mono-domain and this phase will be stable. However when we reduce the system size to thin-films or we work with superlattices formed by the merging of ferro- and para- electric materials (FE,PE), the effect of this cumulative charges is no more negligible.

Imagine that we have a thin film of a ferroelectric material in the polarized phase or that we are studying the interfaces between a FE and a PE material. The discontinuity of the polarization in the surface will create, as we have just reminded, bounded charges of opposite signs. These charges will create an electric field, which is usually called *depolarizing field* that will be generally strong enough to suppress the spontaneous polarization of the material. And making as a consequence this phase non stable.

The system, can present different forms to decrease the effect of the depolarizing charges and thus screening the depolarizing fields that naturally emerge. They are schematized in Fig. 22 and will be studied below.

The most obvious solution if our material is not isolated is to collect the charges formed in the interfaces. This can be done either with a pair of electrodes or having the material surrounded by an adsorbent atmosphere. However, if we consider our system isolated, depending on its concrete characteristics different solutions can appear. We shall discuss them below, doing continuous reference to Fig. 22.

1. The first possible solution is that the polarization rotates pointing through a direction where the material can be thought to be infinite. Which is the same, tangent to the surface where cumulative charges were created. The system under certain mechanical conditions can present this type of solution and remains stable because depolarizing charges are no longer created in the material.
2. Another way to suppress the appearance of the depolarizing charges is to avoid the discontinuity of the polarization. In tri-layer systems formed by merging PE-FE-PE materials such as $(\text{SrTiO}_3\text{-PbTiO}_3\text{-SrTiO}_3)$ where the number of unit cells of the FE material is bigger than those of the PE material, a polarization in the paraelectric phase can emerge eliminating the discontinuity that created the depolarizing charges. If the number of unit cells of the FE material is big enough the system is stable polarizing the PE phase.
3. The most appealing solution for this work to avoid the depolarizing charges is the formation of domains in the FE material. This will create vortex-like and topologically non trivial textures that we shall try to characterize later on.

In this case, the FE material breaks into different domains where the polarization component normal to the surface points in opposite directions. This provokes that the average of the bound charge vanishes and therefore suppress the depolarizing field. The number of domains and hence its size will be determined by the interplay between the energy cost of the domain wall formation and the electrostatic energy of each domain.

Different domain walls can appear as they are pictured in Fig. 21.

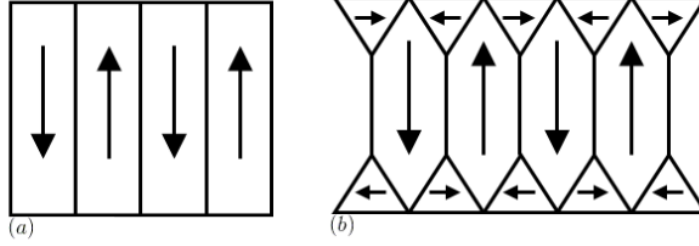


Figure 21: Different domain walls that can arise in FE materials. In (a) Kittel domains and in (b) closure domains.[21]

Closure domains were thought unlikely to appear in ferroelectrics due to the elastic penalty in terms of energy. However, they have been observed and predicted and such domains are the ones that induce vortex patterns.

4. The last solution that the material can present is the suppression of the spontaneous polarization. Cumulative charges will obviously not appear and thus the depolarizing field vanishes. This occurs when all the previous methods fail and can happen for example in tri-layers of PE-FE-PE materials where the number of unit cells of the PE material is bigger than the ones of FE material.

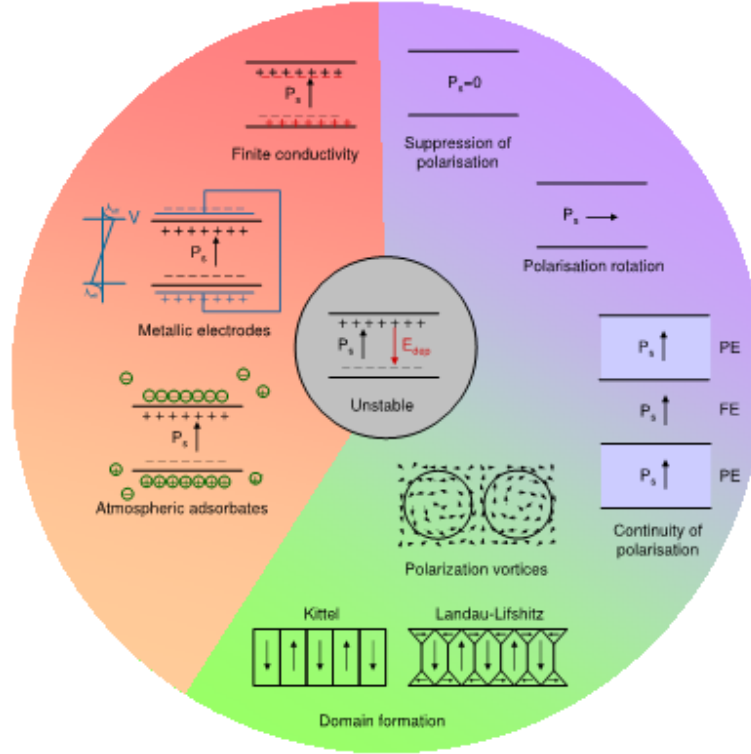


Figure 22: In the middle the depolarizing field that arise from the unscreened bound charges on the surface of the FE material. The left part of the diagram illustrates screening by free charges from metallic electrodes, ions from the atmosphere or mobile charges from within the semiconducting ferroelectric itself. In the right part of the diagram, different ways of preserving the polar state despite the absence of sufficient free charges. One possibility is to form polarization domains that lead to overall charge neutrality on the surfaces. Under suitable mechanical boundary conditions another solution is rotate the polarization plane. Reprinted with permission from [21, 22].

3.2 Ferroelectric bubbles.

Now we shall be interested in finding a system which can be thought as the electric counterpart of magnetic skyrmions.

A perfect candidate is the superlattice combining a ferroelectric perovskite oxide (PbTiO_3) with a dielectric (SrTiO_3). Progress in layer by layer atomic deposition techniques (pulsed laser deposition or molecular beam epitaxy) have allowed the growth of these superlattices

with a control at the atomic level. Hand by hand with these experimental progress, this system is well suited for first-principles [23, 24] and second-principles simulations [18, 25].

The formation of vortex were predicted by second principles calculations and also experimentally detected as it is shown in Fig. 23 leading to chiral objects with an out of plane polarization component that seemed to be easily switchable. All states pictured are degenerated in energy.

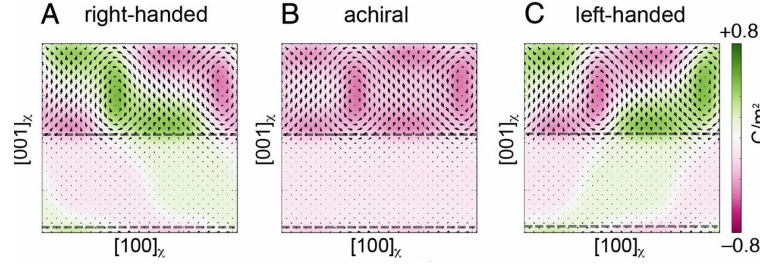


Figure 23: Second principles calculation of electric polarization textures for (SrTiO₃/PbTiO₃). Three different local minima, degenerate in energy. Each texture contains a pair of counterrotated cores yet has different chiral properties. Black arrows indicate the local dipoles, projected onto the (010) plane. A large axial component of the polarization along $\pm[010]$, represented by the green and magenta domains, is observed. Reprinted with permission from [18]

Although the system presents chirality, skyrmionic phases were neither predicted nor experimentally observed within the previous work [18]. We highlight here that our positive components along the z direction are not completely surrounded by negative regions as requested by condition one in Sec. 2, but they form “tubes” with “Z”-like or “S”-like patterns as shown in Fig. 23 A and C respectively.

In order to obtain a system where skyrmionic phases are potentially observable, at least, we shall be requesting that the three conditions stated in Sec. 2 are fulfilled. In particular, this can be accomplished if within a domain of positive polarization for example we induce a negative polarization region. This can be experimentally accessible with AFM microscopy and computationally tested as shown in Fig. 24. In this framework, condition one in Sec. 2 is imposed and therefore it is trivially satisfied, moreover it can be shown that after the relaxation of the matrix the system remains in this metastable state.

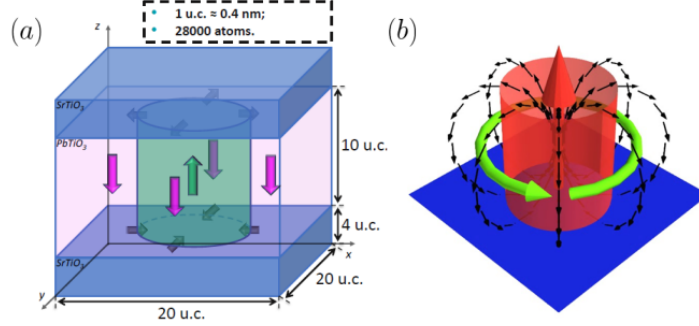


Figure 24: $\text{PbTiO}_3/\text{SrTiO}_3$ superlattices with previously induced polarization by external field .

This system now presents a core where the polarization points upwards and it is surrounded by a polarization that points downwards with a continuous rotating polarization in plane. Which implies that all stated conditions in Sec. 2 are satisfied. The system seems to be the ideal candidate to be the electric analogue of magnetic skyrmion, in following sections we shall try to topologically characterize and deeply study this patterns in order to conclude whether this system is suitable enough to be the electric counterpart of magnetic skyrmions.

3.3 Topological characterization of Ferroelectric bubbles.

In Sec. 2, we have introduced the basic concepts required to perform the topological characterization of magnetic skyrmions. In the remaining of this section we will translate them to the present context.

3.3.1 Order parameter

The order parameter is easily identified with the local electric polarization, defined for every single unit cell in space. Unlike it happens with magnetic spins which are normalized, the local electric polarization is not. From our simulations, the local electric polarization takes a non-zero value throughout the PbTiO_3 column and it is obviously bounded from above. Moreover it is a smooth function in the space. Despite the fact that all the mathematical formalism described in Sec. 2.2 was developed for a vector field that is normalised at every single point in space, it can be trivially generalized to our ferroelectric nanostructure.

Indeed the transformation from a non-normalized to a normalized vector field of our characteristics is a continuous transformation that does not affect its topological properties. More rigorously, the following normalization function is well defined (the norm of the local electric polarization does not vanish at any point in space and so it admit inverse) and smooth.

$$\begin{aligned} \frac{\vec{p}}{||\vec{p}||} : \quad \mathbb{R}^3 &\longmapsto \mathbb{R}^3 \\ (x, y, z) &\longmapsto \frac{\vec{p}(x, y, z)}{||\vec{p}(x, y, z)||} \end{aligned}$$

Finally, to completely justify the transformation, we have to show that the order parameter space after the normalisation transformation is a deformation retract of the order parameter space before the transformation. Hence it has the same topological properties. In order to do that, first we shall see what these spaces look like.

The order parameter space before the transformation can be identified with the solid sphere $\mathbb{D}^3 = \{p_x^2 + p_y^2 + p_z^2 \leq p_{max}\} \setminus (0, 0, 0)$ where the sign \setminus means that we do not consider the point $(0, 0, 0)$ because our polarization never vanishes³.

The order parameter after the transformation is the sphere $\mathbb{S}^2 = \{p_x^2 + p_y^2 + p_z^2 = 1\}$.

The deformation retract is given by the map

$$\begin{aligned} r : \quad \mathbb{D}^3 \setminus (0, 0, 0) &\longmapsto \mathbb{S}^2 \\ \vec{x} &\longmapsto \frac{\vec{x}}{||\vec{x}||} \end{aligned}$$

This is a deformation retract and as a consequence both spaces share the same homotopy type. An scheme of the so-called deformation is pictured in Fig. 25

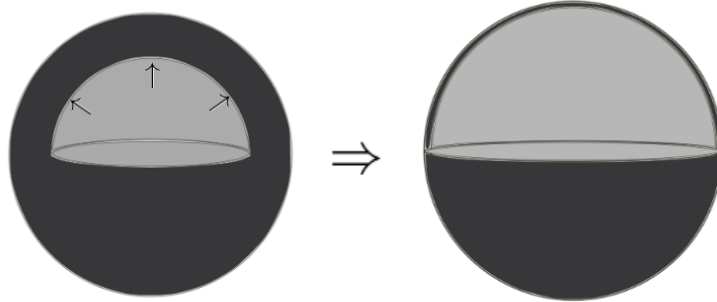


Figure 25: Deformation retract from a spherical shell into a sphere.

³With out loss of generality we can suppose here that $p_{max} > 1$ because, as we are only interested in the topology, spheres of different radius will for us be equivalent

3.3.2 Dimensionality

Once we have justified that normalization is topologically permitted we have an order parameter $\tilde{\vec{p}} = \frac{\vec{p}}{||\vec{p}||}$ that satisfies all the restrictions we gave in Sec. 2. However there is still another difference between the magnetic skyrmions and the ferroelectric bubbles which is the dimensionality of the system. Magnetic skyrmions are two dimensional objects while our FE complex pattern is defined in three dimensions.

However we can study our system layer by layer and compute for each layer the Skyrmion number following the recipe given in Eq.2. We will show that this number is well defined independently from the layer where it is computed and so we can extend the definition of Skyrmion number to such structures.

If we compute the Skyrmion number for each layer taking Eq. (3) we can solve the radial part that is the same for each layer and we arrive to

$$N_{Sk}(z) = \frac{1}{4\pi} \cdot 2 \cdot \Phi(\phi)|_0^{2\pi} = m(z)$$

The key point is that for every single layer the boundary conditions are the same for the radial part: a downward pointing polarization in the matrix and an upward pointing polarization inside the bubble and so the radial part is equivalent.

So in this case in each layer the Skyrmion number coincides with the vorticity m . We only have to show that the vorticity is constant for each layer. To do so, lets consider the following function

$$\begin{aligned} \Psi : \mathbb{R} &\longmapsto \mathbb{Z} \\ z &\longmapsto m_z \end{aligned}$$

This function maps each height z to the vorticity of the vector field defined in the xy -plane at height $z, (m_z)$. As our polarization pattern is smooth everywhere in the three-dimensional space, it is continuous concretely in the z direction and so Ψ is a continuous function defined from a connected space into a topological discrete space such as \mathbb{Z} and thus Ψ must be the constant function. Intuitively, and with the knowledge of Sec. 2.2 the result is not surprising, because m is a topological invariant and continuous functions shouldn't alter its value.

As a consequence, the skyrmion number is invariant and well defined for each layer and we can compute it in each case. In Fig. 26 we can see many traversal cuts through all the *PTO* column. There, we can observe that the Skyrmion number and the vorticity as it was expected are invariant and take the value $N_{sk} = m = +1$ but for each plane we have that γ varies from 0 to π passing through $\frac{\pi}{2}$. We can observe that in both interfaces, the Skyrmions don't present any chirality whereas in the intermediate states it is always *RH*. As we conclude at the end of Sec. 2.2, chirality is not topological and so it is allow to vary even if the change is smooth.

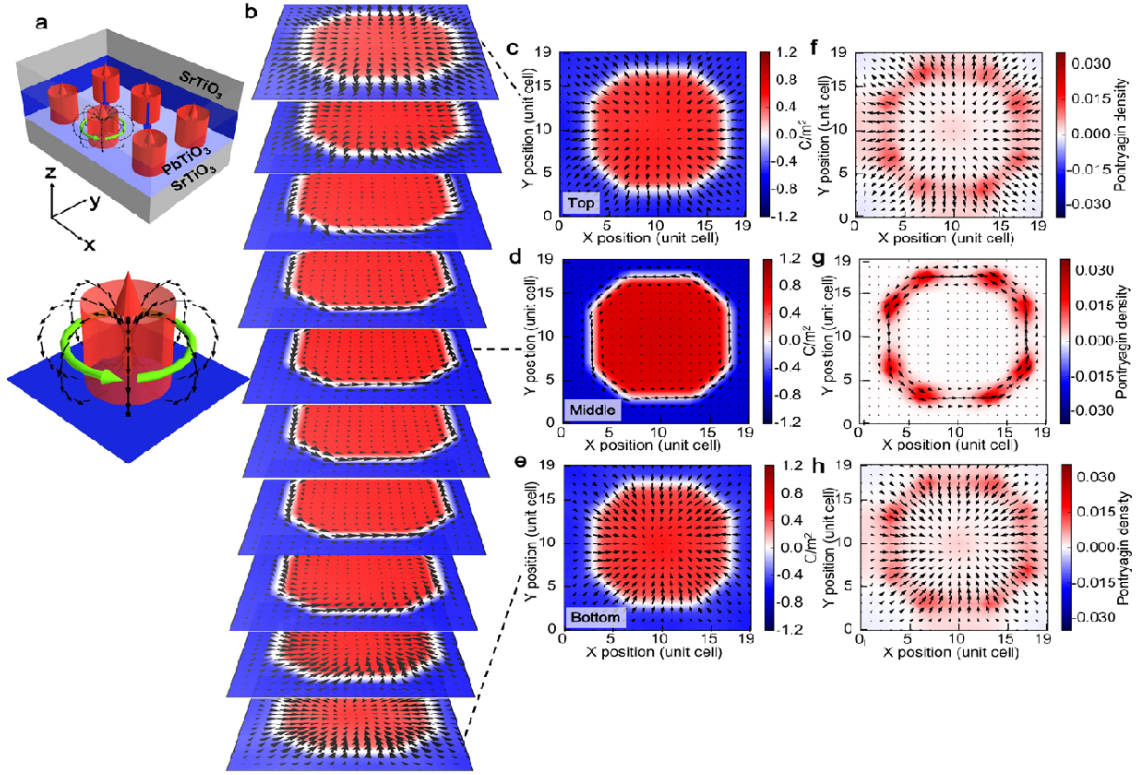


Figure 26: (a) Sketch of the system we are considering and how polarization rotates around the matrix. (b) Different traversal cuts of the *PTO* matrix where we can observe different polarization patterns. (c), (d) and (e) Traversal cuts of the top middle and bottom layers respectively. (f), (g) and (h) Pontryagin density computed for the top, mid and bottom layers.

3.3.3 Chirality

As we discussed in the case of magnetic skyrmions, although chirality is not topological we shall now want to see if our ferroelectric bubbles present or not this property and eventually if it is easily switchable. As we have mention our ferroelectric bubbles present a constant chirality through all layers except in the interfaces where they are not chiral. Obviously, if we change the z component of the polarization through all the matrix of PbTiO_3 , that is changing pointing up polarizations with pointing down and viceversa will change (the Skymion number) and the chirality. However, depending on the matrix size this change might be not possible, we wish to induce a change in the chirality without

changing the z component of our vector field, that is we would like to change the in plane component.

Depending on the shear stress the substrate induce in the PbTiO_3 matrix in-plane polarization changes, as a consequence of this, depending on the shear stress we could end up having either right-handed or left-handed columns.

Although it is not a common idea to apply mechanical fields to switch ferroelectric domains because stress σ or strain ϵ is coupled with electric polarization in even symmetry $-\sigma\vec{p}^2$ or $-\epsilon\vec{p}^2$. It is shown [26] that Gibbs energy presents a dependence on shear stress of the form

$$G \propto -\sigma_{ij}p_k p_l.$$

And thus depending on the shear, if one component of the polarization is fixed by lets say an electric field the other component must flip in order to preserve minimum energy as it is shown in Fig. 27

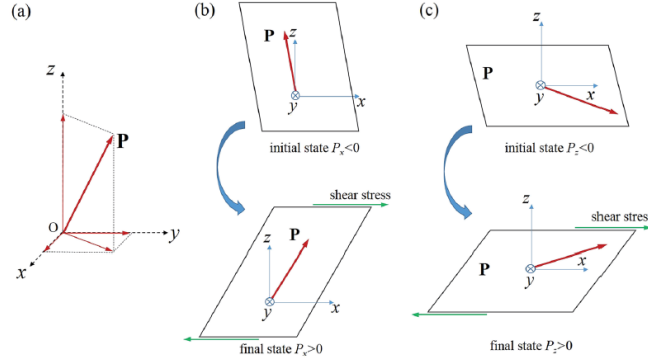


Figure 27: In (a) schematic of a polarization vector in a Cartesian coordinate system. In ((b) and (c)) schematic of two possible switching behaviours of a polarization vector by shear stress.[26]

Now that we know that our objects can present chirality and that it can be determined by the shear stress that our substrate induce on the material, the question should be whether we can control this behaviour and switch chirality to our wish. However this line of investigation will be further explored in future works and not in the present paper.

4 Berry Theory

In this Section we shall develop the Berry theory which is in the base of many novel aspects of the modern condensed matter physics such as quantum Hall effect, modern theory of polarization, magnetic skyrmions and so on.

All the theory is based on the study of the geometrical phase that a system acquires when it performs an adiabatic transformation. In order to introduce this idea we will mention the classical analogous that first motivated Michael Berry to make this theory: the Foucault's pendulum.[27]

4.1 Classical analogous

In this introduction we shall follow some of the ideas treated in [28]. Let us suppose that we have a Foucault pendulum placed on the North pole of a sphere, and that we move it adiabatically (i.e. very slowly) through a geodesic until we reach the equator. Afterwards we move through the equator a certain distance and go back to the North pole by a geodesic(as Fig. 28 schematically shows with the parallel transport of vector in the sphere through a geodesic triangle).

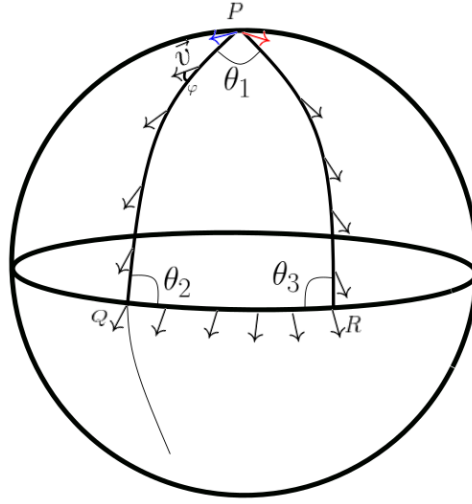


Figure 28: At a given point P , we define a vector \vec{v} that is going to be parallel transported through the sphere. We define the geodesic between P and another point in the sphere, Q . This geodesic is the great circle that passes along these two points. When we move along the geodesic, the vector \vec{v} changes its orientation in such a way that the angle with respect to the geodesic (φ) remains constant. At Q , we follow a second geodesic that connects Q and R and proceed in the same way. Once at R , we close the circuit coming back to P following a third geodesic. If we compare the initial vector (plotted in blue) and the one that arrives after the excursion (plotted in red), they do have the same module, both are contained in a plane tangent to the sphere at P but they form an angle. In other words, its phase has change if we define the vector in polar coordinates.

Geodesics in the sphere are great circles, that divide the sphere in exactly two halves. Moving along a great circle in the sphere is like moving in a straight line in a flat space and hence the plane of oscillation of the pendulum should not rotate. Intuitively, the two halves of the sphere have equal mass and so there is nothing to break symmetry.

Studying this problem is the same as studying the parallel transport of a vector through a surface where we impose two conditions: (i) First, the vector moves such that it remains tangent to the surface; and (ii) second that keeps a constant angle with the path that is making.

If the vector is being parallel transported along a flat surface, then the vector will not accumulate any phase and will return to the initial position unchanged. However when the surface presents some curvature, the vector will develop a phase after travelling around a closed loop as it is pictured in Fig. 28 and Fig. 29.

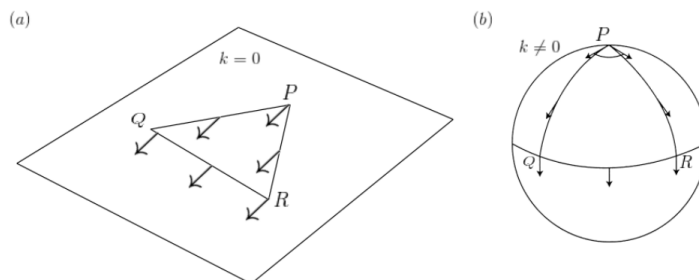


Figure 29: Parallel transport of a vector in different surfaces. (a) Flat surface where the vector accumulates zero change. (b) Curved surface where the change in the vector after a closed loop is patent. k stands for the Gauss curvature of the surface. Adapted with permission from [28]

In fact the change of the vector will be proportional to the integral of the curvature in the surface enclosed by the path, as Gauss-Bonnet formula suggests. As it will be shown in Sec. 4.2 this result will help us later to define a local curvature on our Hilbert space. If a pendulum is adiabatically transported through a geodesic triangle such as in Fig. 28, the changes in the oscillation plane are localized at the vertices of the geodesic triangle (points P , Q and R in Fig. 28). Then the total shift α , will be the sum of the angles $\alpha = \theta_1 + \theta_2 + \theta_3 - \pi$ and by the Gauss-Bonnet formula this equals to $\alpha = \int_S k dS$, where dS is a differential surface element and S is the surface enclosed by the geodesic circuit. However, when the pendulum is on the non-frozen Earth (now we shall consider the usual rotation of the Earth, not only a hypothetical static sphere) at a certain latitude θ_0 the path described as a consequence of the rotation is a circle at a given latitude (a parallel) that it is not a geodesic (unless it is placed on the Equator) but it can be approximated by infinitely many geodesic paths as Fig. 30 suggests.

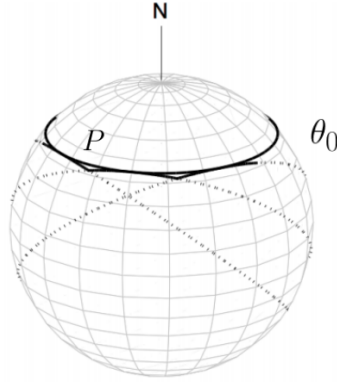


Figure 30: Parallel at a given latitude θ_0 approximated by infinitely many geodesics (great circles) plotted in dashed lines. Adapted with permission from [28].

And thus after a complete turn of the Earth it will be in the initial position. However it shall present a shift with respect to the initial plane of oscillation equals to the solid angle subtended at the centre of the Earth by the cyclic path which turns out to be the classical formula that can be derived with classical mechanics and the Coriolis force $\alpha = 2\pi \sin \theta_0$.

4.2 Quantum mechanics viewpoint.

Let us suppose that we have a hamiltonian that depends adiabatically on a certain parameter λ . This parameter might be atomic displacements in the case for example of modern theory of polarization, or might be the momentum \vec{k} in the quantum hall effect, or the spin positions in the magnetic Skyrmions...

Moreover we are able to diagonalize our hamiltonian for any possible value of λ and thus we can construct a basis of eigenstates [29] [30].

$$H[\lambda(t)] |u_n[\lambda(t)]\rangle = E_n[\lambda(t)] |u_n[\lambda(t)]\rangle$$

As the change is performed adiabatically there is no crossing in the energy levels and so our wave function can be expressed as Eq. 5 states, see Appendix III for a complete derivation.

$$|\psi_n(t)\rangle = e^{\frac{-i}{\hbar} \int_0^t E_n[\lambda(t')] dt'} e^{i\phi_n(t)} |u_n[\lambda(t)]\rangle. \quad (5)$$

Where the first term is usually called the dynamical phase and the second one is known as the geometric phase. Replacing Eq. (5) into the time dependent Schrödinger equation

$i\hbar|\dot{\psi}_n(t)\rangle = H|\psi_n(t)\rangle$, where the dot represents the derivative with respect to time, we arrive to the relation

$$\dot{\phi}_n = i\dot{\lambda} \cdot \langle u_n | \frac{d}{d\lambda} u_n \rangle,$$

where the term

$$A_n(\lambda) \equiv i \langle u_n | \frac{d}{d\lambda} u_n \rangle, \quad (6)$$

is known as the Berry connection. If we perform the integral we arrive to

$$\begin{aligned} \phi_n(t) &= \int_0^t A_n(\lambda) \frac{d\lambda}{dt} dt \\ &= \int_0^{\lambda(t)} A_n(\lambda) d\lambda \end{aligned} \quad (7)$$

Equation (7) contains one of the most important results, the phase variation only depends on the realised path and not in the traversal rate, i.e. it is purely geometric.

It is important to notice that ϕ_n is real because $\langle u_n | \frac{d}{d\lambda} u_n \rangle$ is purely imaginary:

$$\langle u_n | \frac{d}{d\lambda} u_n \rangle + (\langle u_n | \frac{d}{d\lambda} u_n \rangle)^* = \langle u_n | \frac{d}{d\lambda} u_n \rangle + \langle \frac{d}{d\lambda} u_n | u_n \rangle = \frac{d}{d\lambda} \langle u_n | u_n \rangle = 0.$$

However if we select an arbitrary path where $\lambda_i \neq \lambda_f$ because of the fact that our eigenstates have an ill-defined global phase, different selections of gauges will provoke changes in the eigenstates of the type: $|\tilde{u}_n(\lambda)\rangle = e^{-i\beta_n(\lambda)} |u_n(\lambda)\rangle$. These changes will induce different transformations on the Berry connection and hence in the Berry phase.

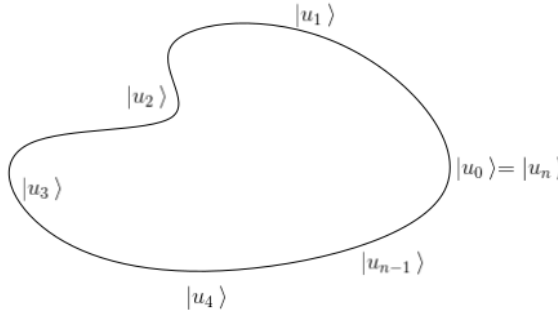
$$\begin{aligned} \tilde{A}_n(\lambda) &= A_n(\lambda) + \frac{d\beta_n}{d\lambda}, \\ \tilde{\phi}_n &= \phi_n + \beta_n(\lambda_f) - \beta_n(\lambda_i). \end{aligned}$$

Making this quantities strongly dependent on the selected gauge and completely ill defined. Eventually we could select a gauge where the geometric phase vanishes and only the dynamical phase remains. Nevertheless, if we now consider a closed path ($\lambda_i = \lambda_f$) we have that both states λ_i and λ_f label the same state and so following the previous notation we have the relations

$$\begin{aligned} |u_n(\lambda_i)\rangle &= |u_n(\lambda_f)\rangle, \\ |\tilde{u}_n(\lambda_i)\rangle &= |\tilde{u}_n(\lambda_f)\rangle. \end{aligned}$$

Imposing those restrictions we have that $\beta_n(\lambda_f) = \beta_n(\lambda_i) + 2\pi l$ where l is an integer and it is called *winding number* of the gauge transformation and so $\tilde{\phi}_n = \phi_n + 2\pi l$. So even considering closed paths ϕ remains being a gauge dependent quantity. Moreover what we have is that depending on the gauge where ϕ is calculated, there is a $2\pi l$ factor to be considered.

This result can also be very easily seen from the discrete approximation of the Berry phase. In this approximation we have that



$$\phi = -\Im (\ln [\langle u_0|u_1\rangle \langle u_1|u_2\rangle \dots \langle u_{n-1}|u_n\rangle])$$

Figure 31: Discretized view of the eigenstates.

Where \Im stands for the imaginary part. And where the restriction $|u_0\rangle = |u_n\rangle$ holds up to a phase. Depending on the selected gauge that relates both eigenstates we will have that ϕ shall present a $2\pi l$ differential factor that arises naturally. It can be proved that in the continuum limit both definitions are the same.

As a conclusion, for a closed path $e^{i\phi_n}$ is gauge invariant which means that it is immutable under gauge transformations and it is well defined. Is hence potentially a physical observable.

In general, our parameter λ might be a vector $\vec{\lambda}$ and so we will define the Berry connection as

$$\vec{A} = i \langle u_n | \vec{\nabla} u_n \rangle \quad (8)$$

On the one hand, in the case where $\vec{\lambda}$ is a 3D-vector we can define the Berry curvature as

$$\vec{\Omega} \equiv \vec{\nabla} \times \vec{A} = i \langle \vec{\nabla} u | \times | \vec{\nabla} u \rangle, \quad (9)$$

and so its components will be

$$\begin{cases} \Omega_x &= -2\Im(\langle \partial_y u | \partial_z u \rangle), \\ \Omega_y &= -2\Im(\langle \partial_z u | \partial_x u \rangle), \\ \Omega_z &= -2\Im(\langle \partial_x u | \partial_y u \rangle). \end{cases}$$

On the other hand, if our parameter $\vec{\lambda}$ is only defined in a $2D$ space the Berry curvature is a scalar and we have the relation.

$$\Omega = \Omega_z = -2Im(\langle \partial_x u | \partial_y u \rangle)$$

Because of the way that the Berry curvature is defined is clearly gauge invariant. Note that even if the eigenstate u is multiplied by a phase, as in Eq. (9) it appears once as bra, and once as ket this phase will cancel out. Moreover remember that the change in the Berry connection was of the form $\vec{A} = A + \nabla\beta$ and as we know it holds that $\nabla \times \nabla\beta = 0$. Stokes theorem makes the link between the definitions of the Berry connection [Eq. (6)] and the Berry curvature [Eq. (9)]

$$\phi_n(C) = \oint_C \vec{A} d\vec{\lambda} = \int_S \vec{\Omega} \cdot \vec{n} dS \equiv \Phi(S), \quad (10)$$

Where S stands for the surface enclosed by the circuit C .

I would like now to clarify a potential doubt that a careful reader could be thinking of. Meanwhile left hand side of Eq. (10) is, as we have said, gauge dependent module 2π . The right hand side of Eq. (10) is defined as an integral of a fully determined gauge independent quantity $\vec{\Omega}$ and is hence gauge independent. It can be proved that if we choose a gauge that is smooth all over the surface S including its boundary C then the equality holds. However, it is true that in general for an arbitrary selection of gauge the equality is only true module 2π .

With this theoretical background our aim now is to explain the origin of our topological invariant, the Skyrmon number. We find the solution in the study of the Chern theorem that states that for any closed surface S without edges it holds

$$\oint_S \vec{\Omega} \cdot \vec{n} dS = 2\pi C,$$

where the integer C is called *Chern number*.

We shall now see that we can relate the integrand of Eq. (2) with the curvature of a Berry phase that is still to be defined. If we do so, we shall be able to identify the skyrmion number with the Chern number, that is $N_{sk} \equiv C$.

4.3 Berry physics of magnetic skyrmions

In the remaining of this Section we shall focus on establish the mentioned relation between the skyrmion number and the Chern number, and study some properties of the Chern

invariants.

The Hamiltonian for a spin under the effect of a magnetic field presents the following form

$$H = \frac{-\gamma B_0 \hbar}{2} \cdot \vec{n} \cdot \vec{\sigma}, \quad (11)$$

where B_0 is the modulus of the applied magnetic field, \vec{n} is the complex skyrmionic spin texture represented in Eq. (1) and $\vec{\sigma}$ the Pauli matrix vector. As we are working with fermions of spin $s = 1/2$ they are 2×2 matrices. Using Eq.(1) and performing the dot product $\vec{n} \cdot \vec{\sigma}$ one obtain

$$\sin \Theta(r) \cos \Phi(\phi) \begin{pmatrix} 0 & 1 \\ 1 & 0 \end{pmatrix} + \sin \Theta(r) \sin \Phi(\phi) \begin{pmatrix} 0 & i \\ -i & 0 \end{pmatrix} + \cos \Theta(r) \begin{pmatrix} 1 & 0 \\ 0 & -1 \end{pmatrix}.$$

finally, the Hamiltonian takes the form

$$H = \frac{-\gamma B_0 \hbar}{2} \cdot \begin{pmatrix} \cos(\Theta(r)) & \sin(\Theta(r))e^{-i\Phi(\phi)} \\ \sin(\Theta(r))e^{i\Phi(\phi)} & -\cos(\Theta(r)) \end{pmatrix}.$$

The Hamiltonian operator depends adiabatically on the position, through the explicit dependence on r and ϕ . Our Hamiltonian matrix (H) satisfies that $\det H = -1$ and $\text{tr}(H) = 0$ and therefore the eigenvalues of the matrix are ± 1 . If we compute the eigenstates we arrive to

$$\begin{aligned} \chi_+(\vec{r}) &= \begin{pmatrix} \cos \frac{\Theta(r)}{2} \\ \sin \frac{\Theta(r)}{2} e^{i\Phi(\phi)} \end{pmatrix}, \\ \chi_-(\vec{r}) &= \begin{pmatrix} \sin \frac{\Theta(r)}{2} e^{-i\Phi(\phi)} \\ -\cos \frac{\Theta(r)}{2} \end{pmatrix}. \end{aligned}$$

Now lets compute the Berry connection and curvature of our two-dimensional spin arrangement for the case where χ_+ is the fundamental level. According to Eq. 6, we have

$$A_0(l) = -i \langle \chi(r) | \partial_l \chi(r) \rangle,$$

where l is a two dimensional vector that stands for the varying position parameter that in our case can take values in the xy plane.

$$\begin{aligned} A_0(l) &= -i \left(\cos \frac{\Theta(r)}{2} \quad \sin \frac{\Theta(r)}{2} e^{-i\Phi(\phi)} \right) \cdot \left(\cos \frac{\Theta(r)}{2} \frac{\partial \Theta}{\partial l} \cdot \frac{1}{2} \cdot e^{i\Phi(\phi)} + i \partial_l \Phi \sin \frac{\Theta(r)}{2} e^{i\Phi(\phi)} \right) \\ &= \sin^2 \frac{\Theta}{2} \cdot \partial_l \Phi = \frac{1}{2} (1 - \cos \Theta) \cdot \partial_l \Phi \end{aligned}$$

If we now compute the Berry curvature $\Omega_z = \partial_x A_y - \partial_y A_x$, we finally obtain

$$\Omega_z = \frac{1}{2r} \sin \Theta \frac{\partial \Phi}{\partial \phi} \frac{\partial \Theta}{\partial r}, \quad (12)$$

which has exactly the same form of the integrand of the Skyrmin number Eq. (2) as it is proven in Appendix I. To be rigorous we have the following relation

$$\oint_S \Omega_z dS = 2\pi N_{sk} = 2\pi C.$$

Thus the skyrmion number and the Chern number are equivalent for our spin system. It is important to notice that this number will obviously depend on the pattern of spins defined on the surface of our order parameter space and not only on the surface itself.

There exists different types of topological invariants. The Euler characteristic for example, which is behind some of the results given in this work (Poincaré-Hopf theorem essentially) depends only on the genus of our surface but it is invariant of the pattern we are considering. The Chern index in contrast is not a characteristic of the surface itself, but of the manifold of eigenstates $|u_n(\lambda)\rangle$ defined over the surface.

In relation with what we have said about Eq. (10) I would like to think of here whether the Chern number is always zero (because Gauss theorem relates our integral with the integral in a volume of the divergence of a curl) or, as we have seen in many examples of Skyrmionic patterns it can take non-zero values. For simplicity and because we are interested in the particular order parameter space of spins in a plane we will consider that $S = \mathbb{S}^2$ i.e. our surface is the unit sphere.

As it is pictured in Fig. 32 we divide our surface in two regions A and B that share the same boundary but with opposite orientations.

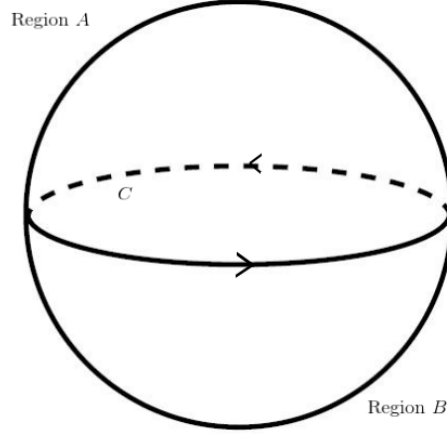


Figure 32: Division of the surface of the sphere in two regions A and B that share the same boundary C .

Dividing the domain of integration we have that

$$\oint_S \Omega \cdot \vec{n} dS = \int_A \Omega \cdot \vec{n} dS + \int_B \Omega \cdot \vec{n} dS$$

Applying Stokes theorem it follows

$$\oint_S \Omega \cdot \vec{n} dS = \oint_C \vec{A}_A d\vec{\lambda} - \oint_C \vec{A}_B d\vec{\lambda}$$

Both integrals measure ϕ_C but a priori in different gauges so its difference would be in general a multiple of 2π .

Only in the case where a global smooth gauge can be defined to all the surface the integral vanish.

As a final note we are now able to explain some of the basic properties that magnetic skyrmions should satisfy and have been recurrent during this work. As we said in Sec. 2 and we emphasized later in Sec. 3 we need to have a region where the out of plane component of our order parameter points in one direction and it is *surrounded* by a region where the out of plane component points oppositely so in particular, regular patterns divided in domains such as the one depicted in Fig. 21(a) should present $N_{sk} = 0$.

We are now able to prove this fact, if we map our pattern to the sphere with the stereographic projection in a similar way as we did in the example Fig. 15 we shall get that

a neighbourhood of the north pole is uncovered because of the fact that we do not have a region covering the rest of the pattern. And so we can define a global gauge in our manifold of eigenstates (for example we can simply get $\begin{pmatrix} \cos \frac{\Theta(r)}{2} e^{-i\Phi(\phi)} \\ \sin \frac{\Theta(r)}{2} \end{pmatrix}$), this gauge is obviously smooth and note that is global because the only point where is not well defined is the north pole $\theta = 0$ where its value $\begin{pmatrix} e^{-i\Phi(\phi)} \\ 0 \end{pmatrix}$ would depend on the directional limit we take. As we can always select a global gauge when this conditions are assumed as a corollary of the previous result we get that their $N_{sk} = 0$.

5 Conclusions

During all this study we have first explained the physical mechanism whereby magnetic skyrmions are created, and afterwards we have characterized their patterns in a topological way. Although theory is not extended to the ferroelectric counterparts in the bibliography, in this work we have set the basis for their topological treatment.

To follow the same order as in magnetic skyrmions we can deduce the following main points.

1. Although there is no ferroelectric interaction to substitute the function that the DM interaction does in the magnetic case, vortex and topologically non trivial textures are formed as a consequence of the depolarizing field and the mechanism to avoid the accumulation of bound charges.
2. Even if the order parameter space is not a sphere \mathbb{S}^2 as in the magnetic case, it admits a transformation that is in fact a deformation retract into the desired sphere and so it share the same homotopy types and are equivalent in the treatment followed in this work.
3. Despite that the dimensionality of our ferroelectric bubbles (3D) is bigger than the magnetic skyrmions (2D) we can consider our system layer by layer, we show that it present a well defined skymion number that is preserved through al the matrix and therefore we can define the skyrmion number of the system to be the skyrmion number of any layer.
4. We have see that our ferroelectric bubbles present chirality. In future works, we shall study whether the handedness of our pattern can be easily switched with an external stimulus.

References

- [1] H. Sagerman. <http://www.3dprintmath.com/figures/5-4>, 2018.
- [2] D. Maccariello, W. Legrand, N. Reyren, K. Garcia, K. Bouzehouane, S. Collin, V. Cros, and A. Fert. Electrical detection of single magnetic skyrmions in metallic multilayers at room temperature. *Nature Nanotechnology*, 13(3):233–237, 2018.
- [3] K. Everschor-Sitte. https://en.wikipedia.org/wiki/Magnetic_skyrmion, 05/09/2018.
- [4] S.S.P. Parkin, M. Hayashi, and L. Thomas. Magnetic domain-wall racetrack memory. *Science*, 2008.
- [5] R. Tomasello and al. A strategy for the design of skyrmion racetrack memories. *Scientific reports*, 2014.
- [6] I. Dzyaloshinsky. A thermodynamic theory of “weak” ferromagnetism of antiferromagnetics. *Journal of Physics and Chemistry of Solids*, 1958.
- [7] T. Moriya. Anisotropic superexchange interaction and weak ferromagnetism. *Physical review*, 1960.
- [8] S. Blundell. *Magnetism in condensed matter*. Oxford university press, 2012.
- [9] Bram van Dijk. *Skyrmions and the Dzyaloshinskii-Moriya Interaction*. Utrecht University. Master thesis., 2014.
- [10] Masaki Uchida and Masashi Kawasaki. Topological Properties and Functionalities in Oxide Thin Films and Interfaces. *Journal of Physics D: Applied Physics*, pages 1–15, 2018.
- [11] N. Nagaosa and Y. Tokura. Topological properties and dynamics of magnetic skyrmions. *Nature Nanotechnology*, 8(12):899–911, 2013.
- [12] N. D. Mermin. The topological theory of defects in ordered media. *Reviews of Modern Physics*, 51(3):591–648, 1979.
- [13] J. Milnor. *Topology from the differentiable viewpoint*. Princeton University Press, 1997.
- [14] J.P. Sethna. Order Parameters, Broken Symmetry, and Topology. 1992.
- [15] A. Dimitrios, Bart S., and B. Jo De. Skyrmion-induced bound states on the surface of 3d topological insulators. *Arxiv*, 2015.

- [16] C. Schuette. <http://www.christophschuette.com/physics/skymions.php>, 05/09/2018.
- [17] N. Reyren, V. Cros, and A. Fert. Magnetic skyrmions: advances in physics and potential applications. *Nature*, 2017.
- [18] P. Shafer, P. Aguado-Puente, P. García-Fernández, A.R. Damodaran, C. Nelson, S. Hsu, J. Wojdel, L. Martin, E. Arenholz, J. Íñiguez, J. Junquera, A. Yadav, and R. Ramesh. Emergent chirality in the electric polarization texture of titanate superlattices. *PNAS*, 2018.
- [19] Nahas et al. Discovery of stable skyrmionic state in ferroelectric nanocomposites. *Nature*, 2015.
- [20] Yadav et al. Observation of polar vortices in oxide superlattices. *Nature*, 2016.
- [21] P. Aguado. *Estudio desde primeros principios de mecanismos de apantallado del campo de depolarización en condensados nanométricos*. Universidad Cantabria, 2011.
- [22] P. Aguado-Puente, J. Junquera, P. Ghosez, J. Tricone, M. Stengel, and C. Lichtensteiger. Ferroelectricity in ultrathin-film capacitors. *Oxide Ultrathin Films: Science and Technology*.
- [23] P. Aguado-Puente and J. Junquera. Structural and energetic properties of domains in pbtio3srtio3 superlattices from first principles. *Physical review B*, 2012.
- [24] P. García-Fernández, P. Aguado-Puente, and J. Junquera. Interplay of couplings between antiferrodistortive, ferroelectric, and strain degrees of freedom in monodomain pbtio3srtio3 superlattices. *Physical review letters*, 2011.
- [25] A. R. Damodaran, J. D. Clarkson, Z. Hong, H. Liu, A. K. Yadav, C. T. Nelson, S. Hsu, M.R. McCarter, K.D. Park, V. Kravtsov, A. Farhan, Y. Dong, P. Aguado-Puente, P. García-Fernández, J. Íñiguez, J. Junquera, R. Ramesh, and L.W. Martin. Phase coexistence and electric-field control of toroidal order in oxide superlattices. *Nature Materials*, 2017.
- [26] W. J. Chen, Shuai Yuan, L.L. Ma, Ye Ji, Biao Wang, and Yue Zheng. Mechanical switching in ferroelectrics by shear stress and its implications on charged domain wall generation and vortex memory devices. *RSC Advances*, 8(8):4434–4444, 2018.
- [27] M. Berry. Classical adiabatic angles and quantal adiabatic phase. *J.Phys. A*, 1985.

- [28] I. Satija. *Butterfly in the quantum world: the story of the most fascinating quantum fractal*. Morgan & Claypool Publishers, 2016.
- [29] M. Berry. Quantal phase factors accompanying adiabatic changes. *Proceedings of the Royal Society of London*, 1985.
- [30] F. Wilczek and A. Shapere. *Geometric phases in physics*. Advanced Series in Mathematical Physics, 2006.
- [31] N. Reyren, V. Cros, and A. Fert. Advances in the physics of magnetic skyrmions and perspective for technology. *Nature Reviews Materials*, 2016.
- [32] J.R. Munkres. *Elements of algebraic topology*. Addison-Wesley Publishing company, 1984.
- [33] J. Lee. *Introduction to topological manifolds*. Springer, 1950.

6 Appendix I: Derivation of basic formulas.

In this appendix we will develop some of the calculus behind Skyrmion number integral and the vector field \vec{n} .

Due to the symmetry of our system (either, ferroelectric dipoles or magnetic spins) it will be useful to work in the following framework.

The direction of the spin shall be denoted by $\vec{n}(\mathbf{r})$ it will be a 3D parameter defined at spacial position $\mathbf{r} = (x, y)$ in polar coordinates and shall be expressed as equation (1) states. The following fundamental relationships shall be needed throughout the derivation

of many concrete parts of this work.

$$\begin{aligned}
x &= r \cos \phi, \\
y &= r \sin \phi, \\
r &= \sqrt{x^2 + y^2}, \\
\phi &= \arctan\left(\frac{y}{x}\right), \\
\frac{\partial r}{\partial x} &= \cos \phi, \\
\frac{\partial r}{\partial y} &= \sin \phi, \\
\frac{\partial \phi}{\partial x} &= -\sin \phi / r, \\
\frac{\partial \phi}{\partial y} &= \cos \phi / r.
\end{aligned}$$

As a consequence of this, the derivatives with respect to x and y , will be computed according to the chain rule theorem as follows

$$\begin{aligned}
\frac{\partial n}{\partial x} &= \frac{\partial n}{\partial r} \cdot \frac{\partial r}{\partial x} + \frac{\partial n}{\partial \phi} \cdot \frac{\partial \phi}{\partial x} \\
&= \frac{\partial n}{\partial r} \cos \phi - \frac{\partial n}{\partial \phi} \sin \phi / r,
\end{aligned} \tag{13}$$

$$\begin{aligned}
\frac{\partial n}{\partial y} &= \frac{\partial n}{\partial r} \cdot \frac{\partial r}{\partial y} + \frac{\partial n}{\partial \phi} \cdot \frac{\partial \phi}{\partial y} \\
&= \frac{\partial n}{\partial r} \sin \phi + \frac{\partial n}{\partial \phi} \cos \phi / r.
\end{aligned} \tag{14}$$

As in many parts of the work we have highlighted, even if our order parameter is three dimensional we are working in a two dimensional frame and as a consequence it has no sense to talk about ∂_z . Throughout this work it will be important to distinguish between the dimension of the magnetic spin or electric polarization vector and the dimensionality of the system itself.

We shall compute now the integrand of the Skyrmon number defined by Tokura as (2).

In order to compute the integrand we first develop the cross product $((\frac{\partial \vec{n}}{\partial x} \times \frac{\partial \vec{n}}{\partial y}))$.

$$\begin{vmatrix}
i & j & k \\
\sin \Phi \sin \Theta \frac{\partial \Phi}{\partial \phi} \sin \phi / r + \cos \Phi \cos \Theta \frac{\partial \Theta}{\partial r} \cos \phi & -\cos \Phi \sin \Theta \frac{\partial \Phi}{\partial \phi} \sin \phi / r + \sin \Phi \cos \Theta \frac{\partial \Theta}{\partial r} \cos \phi & -\sin \Theta \frac{\partial \Theta}{\partial r} \cos \phi \\
-\sin \Phi \sin \Theta \frac{\partial \Phi}{\partial \phi} \cos \phi / r & \cos \Phi \sin \Theta \frac{\partial \Phi}{\partial \phi} \cos \phi / r + \sin \Phi \cos \Theta \frac{\partial \Theta}{\partial r} \sin \phi & -\sin \Theta \frac{\partial \Theta}{\partial r} \sin \phi
\end{vmatrix}$$

Doing the algebra...

$$\begin{aligned}
&\vec{i} \left[\cos \Phi \sin \Theta \frac{\partial \Phi}{\partial \phi} \sin \phi / r \sin \Theta \frac{\partial \Theta}{\partial r} \sin \phi - \sin \Phi \cos \Theta \frac{\partial \Theta}{\partial r} \cos \phi \sin \Theta \frac{\partial \Theta}{\partial r} \sin \phi + \cos \Phi \sin \Theta \frac{\partial \Phi}{\partial \phi} \cos \phi / r \sin \Theta \frac{\partial \Theta}{\partial r} \cos \phi + \sin \Phi \cos \Theta \frac{\partial \Theta}{\partial r} \cos \phi \sin \Theta \frac{\partial \Theta}{\partial r} \sin \phi \right] \\
&\vec{j} \left[\sin \Phi \sin^2 \Theta \frac{\partial \Phi}{\partial \phi} \sin^2 \phi / r \frac{\partial \Theta}{\partial r} + \cos \Phi \cos \Theta \sin \Phi \sin \Theta \cos \phi \frac{\partial \Theta}{\partial r} \frac{\partial \Theta}{\partial r} + \sin \Phi \sin^2 \Theta \frac{\partial \Phi}{\partial \phi} \cos^2 \phi / r \frac{\partial \Theta}{\partial r} - \cos \Phi \cos \Theta \sin \Phi \sin \Theta \cos \phi \frac{\partial \Theta}{\partial r} \frac{\partial \Theta}{\partial r} \right]
\end{aligned}$$

$$\vec{k} \left[\cancel{\sin\Phi \sin\Theta \frac{\partial\Phi}{\partial\phi} \sin\phi / r \cos\Phi \sin\Theta \frac{\partial\Phi}{\partial\phi} \cos\phi / r + \sin^2\Phi \sin\Theta \frac{\partial\Phi}{\partial\phi} \cos\Theta \frac{\partial\Theta}{\partial r} \frac{1}{r}} - \cancel{\sin\Phi \sin\Theta \frac{\partial\Phi}{\partial\phi} \sin\phi / r \cos\Phi \sin\Theta \frac{\partial\Phi}{\partial\phi} \cos\phi / r + \cos^2\Phi \sin\Theta \frac{\partial\Phi}{\partial\phi} \cos\Theta \frac{\partial\Theta}{\partial r} \frac{1}{r}} \right]$$

Rearranging things up we get

$$\begin{aligned} \frac{\partial n}{\partial x} \times \frac{\partial n}{\partial y} &= \left(\cos\Phi \sin^2\Theta \frac{\partial\Theta}{\partial r} \frac{\partial\Phi}{\partial\phi} \frac{1}{r} \right) \vec{i} \\ &+ \left(\sin\Phi \sin^2\Theta \frac{\partial\Theta}{\partial r} \frac{\partial\Phi}{\partial\phi} \frac{1}{r} \right) \vec{j} \\ &+ \left(\sin\Theta \cos\Theta \frac{\partial\Theta}{\partial r} \frac{\partial\Phi}{\partial\phi} \frac{1}{r} \right) \vec{k} \end{aligned}$$

Finally we arrive to the result

$$n \left(\frac{\partial n}{\partial x} \times \frac{\partial n}{\partial y} \right) = \frac{1}{r} \frac{\partial\Theta}{\partial r} \frac{\partial\Phi}{\partial\phi} \sin\Theta \quad (15)$$

Which, as we wanted to prove has the same form as Eq. 12 up to constant factors.

As a final step, we can arrive to a more visual form of the Skyrmin number performing the integral and obtaining

$$\begin{aligned} N_{sk} &= \frac{1}{4\pi} \int \int d^2r \cdot n \cdot \left(\frac{\partial n}{\partial x} \times \frac{\partial n}{\partial y} \right) \\ &= \frac{1}{4\pi} \int_0^\infty \int_0^{2\pi} r dr d\phi \frac{1}{r} \frac{\partial\Theta}{\partial r} \frac{\partial\Phi}{\partial\phi} \sin\Theta = \frac{1}{4\pi} [-\cos\Theta(r)]_0^\infty [\Phi(\phi)]_0^{2\pi} \end{aligned}$$

And hence we have recovered Equation (3). Studying this expression we can see that the term $\cos\Theta(\mathbf{r})$ is only related with the third component of our order parameter and the term in $\Phi(\phi)$ has to do with the in plane component.

Now we will compute the surface integral of $\vec{n}(\vec{\nabla} \times \vec{n})$, as a first step, using all the notation we have shown in this section the reader can easily arrive to

$$\vec{n}(\vec{\nabla} \times \vec{n}) = \sin((m-1)\phi + \gamma) \left[\frac{\partial\Theta}{\partial r} + \sin(2\Theta) \frac{m}{2r} \right] \quad (16)$$

Where we have used some well known relations of the type $\sin\alpha \cos\beta - \cos\alpha \sin\beta = \sin(\alpha - \beta)$. Now lets compute the integral of surface of Eq. (16).

$$\begin{aligned} \int \int \sin((m-1)\phi + \gamma) \left[\frac{\partial\Theta}{\partial r} + \sin(2\Theta) \frac{m}{2r} \right] dx dy &= \int \int \sin((m-1)\phi + \gamma) \left[\frac{\partial\Theta}{\partial r} + \sin(2\Theta) \frac{m}{2r} \right] r dr d\phi \\ &= \int_0^{2\pi} \sin((m-1)\phi + \gamma) d\phi \int_0^\infty \left[\frac{\partial\Theta}{\partial r} + \sin(2\Theta) \frac{m}{2r} \right] r dr \end{aligned}$$

The integral in ϕ is easy to compute and we obtain

$$\int_0^{2\pi} \sin((m-1)\phi + \gamma) d\phi = \begin{cases} \text{if } m \neq 1 & \frac{\cos((m-1)\phi + \gamma)}{(1-m)} \Big|_0^{2\pi} = 0 \\ \text{if } m = 1 & 2\pi \sin(\gamma) \end{cases}$$

And so if we want that the integral of Eq. (16) is non zero we have to impose $m = 1$ and $\gamma \neq k\pi$.

7 Appendix II: DM interaction revisited.

In this section we shall revisit the DM interaction and how depending on the direction of the vector \vec{D}_{ij} some patterns are more stable than others. Just as a remind, our DM Hamiltonian for a pair of spins was of the form

$$\mathcal{H}_{asym} = -\vec{D}_{12} \cdot (\vec{S}_1 \times \vec{S}_2). \quad (17)$$

In the first place, as we said in Sec. 2, we shall analyse the case when the vector \vec{D}_{ij} points in the direction of $\vec{r}_{ij} = \vec{r}_i - \vec{r}_j$ for a pair of spins at positions \vec{r}_i and \vec{r}_j , as it is shown in [Fig. 33(a)].

The Hamiltonian in Eq. (17) refers to the energy of a couple of spins. We hall now take the step towards a continuum model performing a sum over first neighbours. Assuming a square lattice as shown in [Fig. 33(b)].

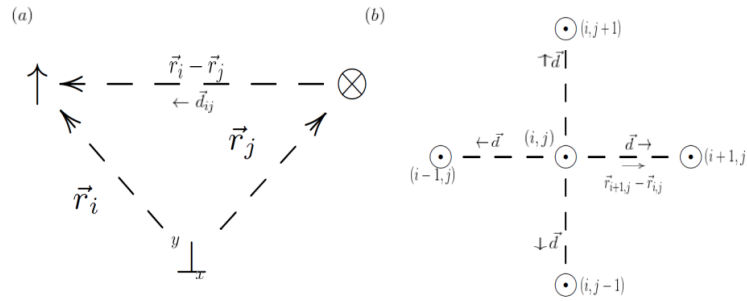


Figure 33: (a) Sketch of how spins align with a given DM vector. (b) Schematic representation of first neighbours and their place in the lattice, vectors \vec{r}_{ij} and \vec{d} as explained above for each site.

In order to do this we will have to compute the sum of the interaction $-\vec{D}_{ij}(\vec{S}_i \times \vec{S}_j)$ to the four neighbour sites giving the following result:

$$\begin{aligned} \mathcal{H}_{asym}(u) = \sum_v^{neigh} \mathcal{H}_{asym}(u, v) = & -\vec{d}_x \cdot (\vec{S}_{ij} \times \vec{S}_{i+1,j}) + \vec{d}_x \cdot (\vec{S}_{ij} \times \vec{S}_{i-1,j}) \\ & -\vec{d}_y \cdot (\vec{S}_{ij} \times \vec{S}_{i,j+1}) + \vec{d}_y \cdot (\vec{S}_{ij} \times \vec{S}_{i,j-1}), \end{aligned}$$

where, as we have said, the interaction vector \vec{d} is in the direction of the vector \vec{r}_{ij} and it has obviously opposite direction for right or left neighbours as explained in Sec. 2. Performing the previous sum we obtain

$$\begin{aligned} \mathcal{H}_{asym}(u) = & -d_x \{S_y(i, j)[S_z(i+1, j) - S_z(i-1, j)] + S_z(i, j)[S_y(i-1, j) - S_y(i+1, j)]\} - \\ & d_y \{S_z(i, j)[S_x(i, j+1) - S_x(i, j-1)] + S_x(i, j)[S_z(i, j-1) - S_z(i, j+1)]\} \end{aligned}$$

If we now approximate by finite differences and we suppose that $d_x = d_y = 1$ (i.e., we normalize the DM vector), we obtain (up to factors two coming for the finite differences approximation that we ignore for the moment) the following expression

$$\mathcal{H}_{asym}(u) = -S_y(i, j)\partial_x S_z(i, j) + S_z(i, j)\partial_x S_y(i, j) - S_z(i, j)\partial_y S_x(i, j) + S_x(i, j)\partial_y S_z(i, j) \quad (18)$$

Knowing that $\nabla \times \vec{S}$ has the form,

$$\partial_y \vec{S}_z \vec{i} - \partial_x \vec{S}_z \vec{j} + (\partial_x \vec{S}_y - \partial_y \vec{S}_x) \vec{k},$$

where we have assumed that since the skyrmion lie in the xy plane it is non-sense to compute derivatives with z . Then Eq. (18) reduces to $\vec{S}(\nabla \times \vec{S})$.

That is the DM Hamiltonian for the interaction between one spin and its first neighbours. To know the full Hamiltonian we have to sum over all the lattice sites.

$$\mathcal{H}_{asym} = \frac{1}{2} \sum_{\langle i, j \rangle} -\vec{D}_{ij}(\vec{S}_i \times \vec{S}_j)$$

The factor 1/2 cancels with the factor 2 of the finite differences approximation. Performing the sum we finally arrive to

$$\mathcal{H}_{asym} = D \vec{S}(\nabla \times \vec{S}),$$

where D is a constant that measure the force of the interaction and we recover the Hamiltonian of [11]. As we have proven in Appendix I that Hamiltonian has the following form for our pattern of spins

$$\mathcal{H}_{asym} = D \sin[(m-1)\phi + \gamma] \left[\frac{\partial \Theta}{\partial r} + \sin(2\Theta) \frac{m}{2r} \right].$$

And, as we can check, the most stable skyrmion is the $m = 1$, $\gamma = \pm \frac{\pi}{2}$ depending on the sign of D , those are, chiral Bloch type Skyrmions as we anticipated in Sec. 2. Its handedness will depend on the sign of the constant D .

Now we shall do the same for the DM interaction where the vector \vec{D}_{ij} is orthogonal to the direction of \vec{r}_{ij} . In this case we shall analyse what happens when the vector \vec{D}_{ij} lies orthogonal to the vector \vec{r}_{ij} as it is pictured in [Fig. 34(a)].

As in the former case we shall compute the overall Hamiltonian performing first a sum over first neighbours for a given site. Assuming the same square lattice as schematically shown in [Fig. 34(b)].

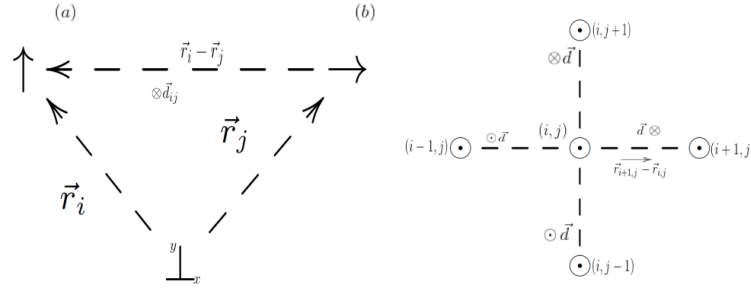


Figure 34: (a) Sketch of how spins align with a given DM vector. (b) Schematic representation of first neighbours and their place in the lattice, vectors \vec{r}_{ij} and \vec{d} as explained above for each site.

$$\begin{aligned} \mathcal{H}_{asym}(u) = \sum_v^{neigh} \mathcal{H}_{asym}(u, v) = & -\vec{d}_y \cdot (\vec{S}_{ij} \times \vec{S}_{i+1,j}) + \vec{d}_y \cdot (\vec{S}_{ij} \times \vec{S}_{i-1,j}) \\ & -\vec{d}_x \cdot (\vec{S}_{ij} \times \vec{S}_{i,j+1}) + \vec{d}_x \cdot (\vec{S}_{ij} \times \vec{S}_{i,j-1}), \end{aligned}$$

where now the vector \vec{D} is perpendicular to the direction of \vec{r}_{ij} . Performing the sum as in the previous example and approximating by finite differences we arrive in a very similar way to

$$\mathcal{H}_{asym}(u) = S_z(i, j) \partial_x S_x(i, j) + S_z(i, j) \partial_y S_y(i, j) - S_x(i, j) \partial_x S_z(i, j) - S_y(i, j) \partial_y S_z(i, j)$$

As in the former case this is the Hamiltonian for the interaction of one spins with its nearest neighbours. Performing the sum to every site we can compute the full Hamiltonian (where factor 2 coming from finite differences approximation cancel as it happened before)

and we obtain the same than in [31] and performing the derivatives we obtain the following expression

$$\mathcal{H}_{asy} = D \cos [(m-1)\phi + \gamma] \left[\frac{\partial \Theta}{\partial r} + \sin(2\Theta) \frac{m}{2r} \right].$$

And as we can check the most stable skyrmion is the $m = 1$, $\gamma = 0, \pi$ depending on the sign of D , those are, Hedgehog non-chiral type skyrmions as we anticipated in Sec. 2.

8 Appendix III: Adiabatic theorem and first steps on Berry theory

In this Appendix we shall explain the starting point for develop Berry theory and prove Eq. 5 with a complete derivation.

An adiabatic transformation is defined by a gradual change of the external conditions in a given process. Typically, there are two times involved. (i) First, we have T_i is the “internal” time, representing the characteristic time of the system itself. (ii) Second, we have T_e is the “external” time over which the parameters of the system change appreciably. In an adiabatic transformation it holds $T_e \gg T_i$. Let us now suppose, that we have a Hamiltonian whose spectrum is discrete and non-degenerate, and it depends on a certain parameters that changes adiabatically. The adiabatic theorem states that if the particle was initially in the n -th state of \mathcal{H}^i it will be carried into the n -th eigenstate of \mathcal{H}^f .

Proof. If the Hamiltonian changes with time, then the eigenfunctions and eigenstates follow the following relation

$$\mathcal{H}(t)\psi_n(t) = E_n(t)\psi_n(t)$$

And in each instant of time they form a complete and orthonormal basis $\langle \psi_n(t) | \psi_m(t) \rangle = \delta_{nm}$. And because they form a complete set, the general solution of the time-dependent Schrödinger equation

$$i\hbar \frac{\partial}{\partial t} \Psi(t) = \mathcal{H}(t)\Psi(t),$$

can be expressed as a linear combination of them

$$\Psi(t) = \sum_n c_n(t) \psi_n(t) e^{i\theta_n(t)}. \quad (19)$$

Replacing Eq. 19 in the time dependent Schrödinger equation we obtain

$$i\hbar \sum_n [\dot{c}_n(t) \psi_n + c_n \dot{\psi}_n + i c_n \psi_n \dot{\theta}_n] e^{i\theta_n} = \sum_n c_n (\mathcal{H} \psi_n) e^{i\theta_n}$$

As $\theta_n(t)$ is the usual phase of temporal evolution and it takes the form:

$$\theta_n(t) \equiv -\frac{1}{\hbar} \int_0^t E_n(t') dt' \Rightarrow \dot{\theta} = -\frac{1}{\hbar} E_n(t)$$

The last term of left hand side and the right hand side cancel out giving rise to

$$\sum_n \dot{c}_n \psi_n e^{i\theta_n} = - \sum_n c_n \dot{\psi}_n e^{i\theta_n}$$

multiplying the last equation by the “bra” $\langle \psi_m |$ and using the orthogonal property of our basis of eigenstates we get

$$\dot{c}_m = - \sum_n c_n \langle \psi_m | \dot{\psi}_n \rangle e^{i(\theta_n - \theta_m)}. \quad (20)$$

We save for the moment this result and now we differentiate the time dependent Schrödinger equation in order to obtain an easier relation for the term $\langle \psi_m | \dot{\psi}_n \rangle$ obtaining

$$\dot{\mathcal{H}} \psi_n + \mathcal{H} \dot{\psi}_n = \dot{E}_n \psi_n + E_n \dot{\psi}_n$$

Proceeding in the same way we multiply by the “bra” $\langle \psi_m |$

$$\langle \psi_m | \dot{\mathcal{H}} | \psi_n \rangle + \langle \psi_m | \mathcal{H} | \dot{\psi}_n \rangle = \dot{E}_n \langle \psi_m | \psi_n \rangle + E_n \langle \psi_m | \dot{\psi}_n \rangle$$

Exploiting now the hermiticity of our Hamiltonian

$$\langle \psi_m | \mathcal{H} | \dot{\psi}_n \rangle = \langle \dot{\psi}_n | \mathcal{H} | \psi_m \rangle = E_m \langle \dot{\psi}_n | \psi_m \rangle = E_m \langle \psi_m | \dot{\psi}_n \rangle$$

And then, it follows that for the case $n \neq m$

$$\langle \psi_m | \dot{\mathcal{H}} | \psi_n \rangle = (E_n - E_m) \langle \psi_m | \dot{\psi}_n \rangle \quad (21)$$

Finally from Eq.20 and Eq. 21 we get

$$\dot{c}_m(t) = -c_m \langle \psi_m | \dot{\psi}_m \rangle - \sum_{n \neq m} c_n \frac{\langle \psi_m | \dot{\mathcal{H}} | \psi_n \rangle}{E_n - E_m} e^{(-i/\hbar) \int_0^t [E_n(t') - E_m(t')] dt'}.$$

And now we apply the adiabatic approximation where we assume that $\dot{\mathcal{H}}$ is extremely small and thus can be neglected obtaining

$$\dot{c}_m(t) = -c_m \langle \psi_m | \dot{\psi}_m \rangle$$

whose solution is of the type

$$c_m(t) = c_m(0)e^{i\phi_m(t)},$$

where $\phi_m(t) = i \int_0^t \langle \psi_m(t') | \frac{\partial}{\partial t'} \psi_m(t') \rangle dt'$ turns out to be the Berry phase.

Therefore if $c_n(0) = 1$ y $c_m(0) = 0$ for every $m \neq n$ the particle remains in the n -th state. \square

As a conclusion we obtain that two phases naturally arises in the evolution of an adiabatic process, one of them is the usual dynamic phase which has to do with the Hamiltonian and is independent of the geometry of the path traversed and another one that is purely geometric and is the analogue to the geometric phase arising in the Foucault Pendulum because of the nonholonomic process.

Now that Eq. (5) is fully explained we replace it in the time dependent Schrödinger equation and we obtain

$$\begin{aligned} & \cancel{E_n(\lambda(t)) \cdot e^{-\frac{i}{\hbar} \int_0^t E_n(\lambda(t')) dt'}} e^{i\phi_n(t)} |u_n(\lambda(t))\rangle + i\hbar e^{-\frac{i}{\hbar} \int_0^t E_n(\lambda(t')) dt'} i \cdot \dot{\phi}_n e^{i\phi_n(t)} |u_n(\lambda(t))\rangle + \\ & + i\hbar e^{-\frac{i}{\hbar} \int_0^t E_n(\lambda(t')) dt'} e^{i\phi_n(t)} \cdot \dot{\lambda} \left| \frac{du_n}{dt} \right\rangle = \cancel{E_n(\lambda(t)) \cdot e^{-\frac{i}{\hbar} \int_0^t E_n(\lambda(t')) dt'}} e^{i\phi_n(t)} |u_n(\lambda(t))\rangle \end{aligned}$$

Rearranging things up we arrive to the following expression

$$i \cdot \dot{\phi}_n |u_n\rangle = -\dot{\lambda} \left| \frac{du_n}{dt} \right\rangle$$

Multiplying each side by the bra $\langle u_n |$ we finally obtain

$$\dot{\phi}_n = i \dot{\lambda} \langle u_n | \frac{du_n}{dt} \rangle$$

As a final note to this Appendix, we shall obtain the relations for the Berry curvature. We shall do it step by step for Ω_x being equivalent for the rest of components.

Taking Eq. (9) as a reference we have that

$$\Omega_x = (\partial_y A_z - \partial_z A_y) = \partial_y (i \langle u_n | \partial_z | u_n \rangle) - \partial_z (i \langle u_n | \partial_y | u_n \rangle)$$

Expanding the previous relation we obtain

$$\begin{aligned} \Omega_x &= i \langle \partial_y u_n | \partial_z u_n \rangle + \cancel{i \langle u_n | \partial_y \partial_z u_n \rangle} \\ &\quad - i \langle \partial_z u_n | \partial_y u_n \rangle - \cancel{i \langle u_n | \partial_z \partial_y u_n \rangle} \\ &= i \langle \partial_y u_n | \partial_z u_n \rangle - i \langle \partial_y u_n | \partial_z u_n \rangle^* = -2\Im \langle \partial_y u_n | \partial_z u_n \rangle \end{aligned}$$

What proves the relations used in Sec. 4.

9 Appendix IV: Maths underneath.

In this section we shall introduce some of the basic theory related with topology, and more concretely with homotopy. We shall be focusing in basic definitions and useful results that help us to understand basic concepts developed in this work, most of these results are not going to be proved here but can be easily found in for example [32, 33]

Algebraic topology starts with the purpose of establish a functorial link between the category of topological spaces and the category of groups. That is to say to relate topology and algebra. In that way we shall correspond every topological space with a group, to every continuous mapping a homomorphism. With this identification a necessary condition for two spaces being homeomorphic is that their homotopy groups are isomorphic.

Definition 9.1. Let X be a topological space. A *path* in X is a continuous mapping $\gamma : [0, 1] \rightarrow X$. If $\gamma(0) = \gamma(1)$ we say that γ is a *loop*.

We define as *product* or *concatenation* of γ and δ as the path.

$$\gamma * \delta(s) = \begin{cases} \gamma(2s) & 0 \leq s \leq 1/2 \\ \delta(2s - 1) & 1/2 \leq s \leq 1 \end{cases}$$

As we have been discussing in this work we would like to know when two paths are comparable. In order to establish this relation the concept of homotopy appears.

Definition 9.2. Let $\gamma, \delta : [0, 1] \rightarrow X$ be two paths in a topological space X . We shall say that γ is homotopic to δ relative to $\{0, 1\}$ if there exists a continuous mapping $H : [0, 1] \times [0, 1] \rightarrow X$ that satisfies:

1. $H(s, 0) = \gamma(s), \forall s \in [0, 1]$
2. $H(s, 1) = \delta(s), \forall s \in [0, 1]$
3. $H(0, t) = \gamma(0) = \delta(0)$
4. $H(1, t) = \gamma(1) = \delta(1)$

Definition 9.3. In general we would say that two mappings f and g are homotopic relative to the subset $A \subset X$ if there exist a continuous function such that

$$\begin{aligned} F : X \times [0, 1] &\rightarrow Y \\ F(x, 0) &= f(x) \quad \forall x \in X \\ F(x, 1) &= g(x) \quad \forall x \in X \\ F(a, t) &= f(a) = g(a) \quad \forall a \in A, \quad \forall t \in [0, 1] \end{aligned}$$

Path-homotopy is a particular case of the former definition where $A = \{0, 1\}$ and f and g are paths in X .

It can be easily proved that the relation being homotopic defines an equivalence relationship in the set of paths with origin x_0 and end x_1 . With that property we can already define the fundamental homotopy group as follows.

Definition 9.4. Let X be a topological space and lets fix $x_0 \in X$. We shall denote $\pi_1(X, x_0)$ to the set of equivalence classes $[\gamma]$ given by the previous relationship of loops γ in X with base in x_0 .

Given two elements $[\gamma], [\delta] \in \pi_1(X, x_0)$ we define $[\gamma] \cdot [\delta] = [\gamma * \delta]$. This operation gives $\pi_1(X, x_0)$ a group structure whose neutral element is $e_{x_0}(s) = x_0$ the constant loop and the inverse of a path $\gamma(s)$ is $\gamma(s)^{-1} = \gamma(1 - s)$.

If our topological space X is path-connected the group is independent of the base point and so we shall talk about $\pi_1(X)$.

Definition 9.5. Let X and E be two topological spaces. A continuous mapping $p : E \rightarrow X$ is a *covering* if verifies:

1. p is surjective
2. For all $x \in X$ there exist a neighbourhood $x \in U \subset X$ such that $p^{-1}(U) = \bigcup_{i \in I} V_i$ where the V_i are open sets in E that satisfies $V_i \cap V_j = \emptyset$ and $p|_{V_i} : V_i \rightarrow U$ is a homomorfism.

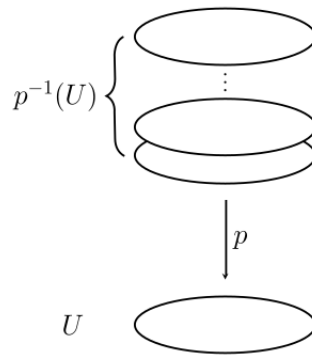


Figure 35: Figure obtained from https://en.wikipedia.org/wiki/Covering_space

We say that the covering is a *universal covering* if the space E is simply connected. For this work we are specially interested in the covering of \mathbb{S}^1 the standard one is the following.

Example 9.1. We have that the following function is a covering:

$$\begin{aligned} p : \mathbb{R} &\longmapsto \mathbb{S}^1 \\ t &\longmapsto (\cos 2\pi t, \sin 2\pi t) \end{aligned}$$

In order to see this as every point is equivalent is enough to prove that there exists a neighbourhood of $(1,0)$ that satisfies the properties of the definition.

We claim $U = \{(\cos 2\pi\theta, \sin 2\pi\theta) : -\frac{1}{4} \leq \theta \leq \frac{1}{4}\}$. Then we have that $p^{-1}(U) = \bigcup_{n \in \mathbb{Z}} (-\frac{1}{4} + n, \frac{1}{4} + n)$ that fulfil all desired conditions. Note that all fibers are infinite.

Definition 9.6. Given a covering $p : E \rightarrow X$ and a continuous application $f : Y \rightarrow X$ a *lifting* of f is a continuous mapping $\tilde{f} : Y \rightarrow E$ such that makes commutative the following diagram $p \circ \tilde{f} = f$

$$\begin{array}{ccc} & & E \\ & \nearrow \tilde{f} & \downarrow p \\ Y & \xrightarrow{f} & X \end{array}$$

Now we shall consider the following result that studies the uniqueness of the lifting.

Proposition 9.1. Let $p : E \rightarrow X$ a covering and $f : Y \rightarrow X$ a continuous mapping. Let $x_0 \in X$, $y_0 \in Y$ and $e_0 \in E$ such that $f(y_0) = x_0 = p(e_0)$. If Y is connected and there exists a lifting \tilde{f} of the function f such that $\tilde{f}(y_0) = e_0$ then \tilde{f} is unique.

Definition 9.7. Let $p : E \rightarrow X$ a covering function let $x_0 \in X$ and $e_0 \in p^{-1}(x_0)$ a point in the fiber of x_0 . We define the function

$$\begin{aligned} \Phi : \pi_1(X, x_0) &\longmapsto p^{-1}(x_0) \\ [\sigma] &\longmapsto \tilde{\sigma}(1) \end{aligned}$$

where $\tilde{\sigma}(1)$ is the lifting of σ with $\tilde{\sigma}(0) = e_0$.

Proposition 9.2. Let's suppose X is path-connected. Then

1. E is path-connected $\iff \Phi$ is surjective.
2. E is simply connected $\iff \Phi$ is bijective.

With all this knowledge we can prove that $\pi_1(\mathbb{S}^1) = \mathbb{Z}$.

Example 9.2. Lets compute the fundamental group of the unit circumference.

We consider the universal covering $p : \mathbb{R} \rightarrow \mathbb{S}^1$ given in Example 9.1. As \mathbb{R} is simply connected there is a bijection between $\pi_1(\mathbb{S}^1, x_0)$ and $p^{-1}(x_0)$. We saw in Example 9.1 that the fiber of each point is $p^{-1}(x_0) = \mathbb{Z}$. So, to conclude the result we only have to show that $\Phi : \pi_1(\mathbb{S}^1) \rightarrow \mathbb{Z}$ is a group homomorphism.

$\Phi([\sigma] \cdot [\tau]) = \Phi([\sigma]) + \Phi([\tau])$. In order to prove this let $X_0 = (1, 0)$. Let $\tilde{\sigma}$ and $\tilde{\tau}$ the lifting of σ and τ to paths in \mathbb{R} with $\tilde{\sigma}(0) = \tilde{\tau}(0) = 0$.

If $n = \tilde{\sigma}(1)$ and $m = \tilde{\tau}(1)$ then we have that $\Phi([\sigma]) + \Phi([\tau]) = n + m$.

Now we have to compute $\Phi([\sigma][\tau]) = \Phi([\sigma\tau])$. However, we have that $\widetilde{\sigma * \tau} = \tilde{\sigma} * \tilde{\tau}^*$, where $\tilde{\tau}^*$ is the lifting of τ with origin in $\tilde{\sigma}(1) = n$.

Then we conclude that Φ is a bijective group homomorphism and so it is an isomorphism and $\pi_1(\mathbb{S}^1) = \mathbb{Z}$.

We shall now want to generalize the idea of the fundamental homotopy group, in order to do this lets see the following results of what is known by topological degree theory.

Definition 9.8. Let $h : \mathbb{S}^1 \rightarrow \mathbb{S}^1$ a continuous application. Let h_* denote the application between the fundamental groups induced by h , that is:

$$\begin{array}{ccc} h_* : \pi_1(\mathbb{S}^1, b_0) & \longmapsto & \pi_1(\mathbb{S}^1, h(b_0)) \\ 1 & \longmapsto & d \end{array}$$

we say that $h_*(1) = d$ is the *degree* of h .

Proposition 9.3. Two mappings $h_1 : \mathbb{S}^1 \rightarrow \mathbb{S}^1$ and $h_2 : \mathbb{S}^1 \rightarrow \mathbb{S}^1$ are homotopic if and only if they have the same degree.

From the last result we deduce that there is a bijection between the homotopy classes of functions $f : \mathbb{S}^1 \rightarrow \mathbb{S}^1$ and \mathbb{Z} . We can understand $\pi_1(X, x_0)$ as the set of homotopy classes relative to x_0 of applications from \mathbb{S}^1 to X .

This allows us to generalize the fundamental homotopy group to the n -th homotopy group of X and denote it by $\pi_n(X, x_0)$ as the set of homotopy classes of applications from \mathbb{S}^n to X that maps $b_0 \in \mathbb{S}^n$ to x_0 .

As we had in the case of $n = 1$:

1. $\pi_n(\mathbb{S}^n) = \mathbb{Z}$.
2. Every continuous application $h : X \rightarrow Y$ induces a homomorphism between their n -th homotopy groups.
3. Given $h_1, h_2 : \mathbb{S}^n \rightarrow \mathbb{S}^n$. They are homotopic if and only if they have the same degree.